



## A method for tachometer-free and resampling-free bearing fault diagnostics under time-varying speed conditions

Huan Huang\*, Natalie Baddour, Ming Liang

*Department of Mechanical Engineering, University of Ottawa, Ottawa, Ontario K1N 6N5, Canada*



### ARTICLE INFO

#### Article history:

Received 7 August 2018

Received in revised form 18 October 2018

Accepted 19 October 2018

Available online 22 October 2018

#### Keywords:

Bearing fault diagnosis

Time-varying speed

Tachometer-free

Oscillatory behavior-based signal

decomposition

Identification of true instantaneous shaft rotational frequency

### ABSTRACT

Bearings often operate under time-varying rotational speed conditions. Processing the signal in the time-frequency domain and extracting the Instantaneous Fault Characteristic Frequency (IFCF) and the Instantaneous Shaft Rotational Frequency (ISRF) are important approaches for bearing fault diagnosis under time-varying speed conditions without signal resampling and without using a tachometer. However, there are two problems: (1) the collected bearing signal is often contaminated by random noise and interferences transmitted from other components, which affects the accuracy of the extracted IFCF, and (2) the ISRF cannot always be found in the Time-Frequency Representation (TFR) of the extracted bearing fault transients, which impacts the accuracy of fault identification. Therefore, a new tachometer-free and resampling-free method is proposed for bearing fault diagnosis under time-varying speed conditions which consists of three main steps: (1) bearing fault signature extraction via Oscillatory Behavior-based Signal Decomposition (OBSD) to suppress the influence of random noise and interferences, (2) IFCF and ISRF estimation via applying a IFCF&ISRF search algorithm to the TFR of the decomposed signal, and (3) automatic bearing fault identification based on the average curve-to-curve ratios of the searched IFCF and ISRF. The IFCF&ISRF search algorithm is proposed based on the analysis of the frequency characteristics of bearing vibration signals. The algorithm can estimate the ISRF even if it is not present in the extracted bearing fault signature. The effectiveness of the proposed method is validated using both simulated signals and experimental data.

© 2018 Elsevier Ltd. All rights reserved.

### 1. Introduction

Bearing fault diagnosis at constant rotational speed has been widely explored [1–7]. For bearing vibration signal analysis, it is known that a local defect in a bearing induces an impulse response when the defect is struck and these impulse responses appear at a certain frequency called the Fault Characteristic Frequency (FCF) [1,2]. Each type of bearing fault has a specific FCF, which is proportional to the rotational frequency [3]. The ratio of the FCF to the rotational frequency, also called fault characteristic order or fault characteristic coefficient, can be determined by the structural parameters of the bearing [4], hence enabling bearing faults to be easily detected and diagnosed in the frequency domain. However, in reality rotating machines often operate under time-varying speed conditions which leads to a time-varying FCF. Under such circumstances, bearing faults cannot be directly diagnosed in the frequency domain.

For bearing fault diagnosis under time-varying FCF, order tracking is one of the conventional methods used to handle the time-

varying speed. By sampling the signal at constant angular (order) increments instead of constant time increments, the time-varying FCF is converted into constant order features [8]. With the resampled signal, fault diagnosis can then be achieved in the order domain according to the fault characteristic order [9]. The implementation of order tracking requires extra instruments, such as tachometers, and also additional computational operations [10], such as signal interpolation. However, tachometers are not always available or feasible to be installed on every machine of interest, and additionally the accuracy of order tracking is limited by interpolation [11]. Therefore, it is important to develop tachometer-free and resampling-free methods for bearing fault diagnosis under time-varying speed conditions.

Resampling-free methods for bearing fault diagnosis under time-varying speed conditions have been investigated based on time-frequency analysis. With the development of time-frequency analysis techniques, such as the Short-Time Fourier Transform (STFT) and wavelet transform, the instantaneous frequency can be shown in a Time-Frequency Representation (TFR) [12]. For a given bearing fault induced signal, the Instantaneous Fault Characteristic Frequency (IFCF) and its harmonics can be observed as Time-Frequency (T-F) curves, also called ridges, in

\* Corresponding author.

E-mail address: [hhuan061@uottawa.ca](mailto:hhuan061@uottawa.ca) (H. Huang).

the TFR. Therefore, bearing faults can be diagnosed without signal resampling by extracting/estimating the IFCF and its harmonics from the TFR. For example, the Iterative Generalized Demodulation (IGD) employs generalized demodulation to convert a curve in the TFR of a signal into a straight line [13], and then iteratively applies generalized demodulation to obtain an order spectrum for fault diagnosis without signal resampling [14]. Following this idea, the IFCF was estimated by taking the point of maximum amplitude at each instant in the TFR, the IFCF was straightened via generalized demodulation, and finally harmonics of the IFCF were straightened iteratively [15]. However, the estimated IFCF may not be accurate since the point of maximum amplitude can be some other frequency component such as the Instantaneous Shaft Rotational Frequency (ISRF) or a low harmonic of the IFCF. To improve the local maximum method, an amplitude sum-based method was proposed to extract the IFCF from the TFR [16]. However, under some circumstances, the ISRF and its harmonics can be more significant in the TFR than the ISRF and its harmonics. Therefore, resampling-free methods for bearing fault diagnosis under time-varying speed condition require a reliable IFCF estimation algorithm.

Similarly, tachometer-free methods for bearing fault diagnosis under time-varying speed conditions rely on the estimation of the ISRF. In [17], the ISRF was estimated by finding the point with local maximum amplitude at each instant. With the estimated ISRF, the signal can be resampled without tachometer measurement of the shaft rotational speed. However, the estimated ISRF may not be accurate via the local maximum amplitude method if the signal is blurred by noise. Therefore, a cost function based method was employed to extract the ISRF for tachometer-free order tracking [18]. The cost function based method was related to both the amplitude of the point and the frequency difference between two connected points, which proved to be more reliable than the local maximum amplitude. All these methods for instantaneous frequency extraction are based on the assumption that the extracted T-F curve is known to be a certain harmonic of the ISRF or the IFCF. However, the extracted T-F curve could be any of them. Therefore, again, it is necessary to develop a more reliable method for T-F curve extraction without the above assumption. Moreover, the collected bearing signal is often contaminated by random noise and interferences transmitted from other sources which need to be removed to ensure the accuracy of the ISRF and IFCF estimation.

For any fault diagnosis approach to work as intended, it is critical to eliminate interferences and noise from the signal prior to the application of the fault diagnosis strategy. Many strategies for the elimination of interference and noise have been proposed in the literature. Band-pass filtering and reference based filtering are commonly used for bearing signal denoising and interference cancellation. Spectral Kurtosis (SK) is a useful technique developed for bearing signal denoising to determine the optimal band-pass filter, since the bearing fault-induced signal has a relatively high resonance frequency [19,20]. However, the interference cannot be removed via spectral kurtosis if the interference has a high frequency or if the frequency of the interference is time-varying and crosses the frequency of the signal of interest. Therefore, an adaptive filter which utilizes the Least Mean Square (LMS) algorithm was proposed to remove the interference for bearing fault diagnosis under time-varying speed conditions [21]. The filter can adaptively estimate the interference signal according to the reference signal correlated to the interference. By subtracting the estimated interference signal from the raw signal, the bearing fault signature can be obtained. However, a reference signal correlated to the interference is not always available. Therefore, frequency-independent and reference-free methods for

bearing fault signature extraction under time-varying speed conditions are of interest to explore.

Instead of decomposing the signal into different frequency bands, new techniques such as Oscillatory Behavior-based Signal Decomposition (OBSD) that decompose a signal according to oscillatory behavior [22] are potentially useful for bearing fault signature extraction under time-varying speed conditions. The OBSD can be used to effectively extract the bearing fault signature from a signal blurred by interferences since the bearing fault signature can be considered as low oscillatory and the interference can be considered as high oscillatory [23]. An iterative OBSD method was developed to remove multiple sets of interferences for bearing fault diagnosis [24]. Additionally, an auto-OBSD method was developed to automatically select parameters related to the OBSD for bearing fault signature extraction [25]. However, to date, the OBSD has only been applied for bearing signature extraction under constant speed conditions. Theoretically, the OBSD method should still be effective under time-varying speed conditions since the oscillatory behavior of the bearing fault signature and interference remain unchanged.

In view of all the above, there are two challenges for the realization of tachometer-free and resampling-free bearing fault diagnosis under time-varying speed conditions: (1) reliable bearing fault signature extraction and (2) reliable IFCF and ISRF estimation. Novel approaches to both these challenges are proposed in this paper. The frequency and oscillatory features of the bearing vibration signal are analyzed. Frequency feature analysis provides necessary information for IFCF and ISRF estimation, and oscillatory feature analysis helps to separate the bearing fault signature from the contaminated signal. Based on the analyses, a resampling-free and tachometer-free methodology is proposed for bearing fault diagnosis under time-varying rotational speed conditions. The proposed method begins with using the OBSD, which is frequency independent and reference-free, to extract the bearing fault signatures from a contaminated signal. Then, an IFCF & ISRF search algorithm is developed to estimate the IFCF and ISRF from the TFR of the decomposed signal. Finally, fault identification is conducted by matching the average curve-to-curve ratio of the estimated IFCF/ISRF to the Fault Characteristic Coefficient (FCC). The effectiveness of the proposed method is validated by simulations and experiments. The remainder of the paper is structured as follows. In Section 2, the frequency and oscillatory features of the bearing vibration signal are analyzed. In Section 3, the proposed bearing fault diagnosis method is presented. Simulations are then conducted to examine the effectiveness of the proposed method in Section 4. In Section 5, signals collected from experiments are used to further test the effectiveness of the proposed method. Finally, in Section 6, conclusions are drawn based on the results in Sections 4 and 5.

## 2. Frequency and oscillatory features of bearing vibration signal

To improve the accuracy of the estimation of the IFCF and ISRF for tachometer-free and resampling-free bearing fault diagnosis, frequency features of the bearing vibration signal under different conditions are summarized in this section. It is important to understand and analyze the key features of a bearing vibration signal under time-varying speed in order for these features to be exploited for fault detection and identification.

### 2.1. Frequency features of bearing vibration signal

Whether under constant speed or time-varying speed conditions, bearing faults can be identified according to the FCF. For a

bearing with outer race fixed and inner race rotating, the FCF of an outer race fault and an inner race fault can be found via

$$\text{BPFO} = \frac{n_b}{2} \left( 1 - \frac{d}{D} \cos \phi \right) f_r \quad (1)$$

$$\text{BPFI} = \frac{n_b}{2} \left( 1 + \frac{d}{D} \cos \phi \right) f_r \quad (2)$$

where  $n_b$  is the number of rolling elements,  $d$  is the diameter of the rolling element,  $D$  is the pitch diameter of the bearing,  $\phi$  is the angle of the load from the radial plane, and  $f_r$  is the shaft rotational frequency. The bearing fault-induced signal is considered as amplitude demodulated, therefore, it is more common to observe the FCF and its harmonics in the envelope spectrum, i.e. the frequency spectrum of the demodulated envelope signal [4]. The Hilbert Transform is commonly used for signal demodulation and the Fourier Transform is used to obtain the frequency spectrum. As shown in Eqs. (1) and (2), the FCF is proportional to the shaft rotational frequency. Without measuring the shaft rotational frequency with a tachometer, it is necessary to estimate the shaft rotational frequency in order to diagnose bearing faults.

To realize bearing fault diagnosis without using tachometers, it is important to understand the peak frequencies in the frequency domain of the collected vibration signal with different faults under different situations. In this section, the frequency features of a bearing vibration signal with different faults are discussed. Localized faults on the inner or outer race are two common faults in bearings. Therefore, the discussion focuses on these two types of faults. Additionally, in reality, the operational condition of a machine is not ideal; problems such as unbalance and misalignment usually exist. In view of this, the frequency features of the vibration signal caused by unbalance and misalignment are also discussed. Also, an interference signal transmitted from other mechanical components such as a gearbox can be also contained in the collected vibration signal. A summary of the peak frequencies of the frequency and envelope spectrum of the vibration signal generated by different situations mentioned above is given in **Table 1**.

**Unbalance:** the unbalanced mass causes an unbalance force in the vibration system. The peak frequencies in the frequency spectrum of the vibration signal generated by unbalance are the shaft rotational frequency, noted as  $1\times$ , and its low harmonics, such as  $2\times$  and  $3\times$  [26].

**Misalignment:** misalignment includes parallel misalignment and angular misalignment. The peak frequencies in the frequency spectrum of the vibration signal generated by misalignment are also  $1\times$  and its low harmonics. Under some specific conditions with angular misalignment, the peak frequencies could be twice the shaft

rotational frequency  $2\times$ , and its low harmonics, since the shaft stiffness varies with rotational angle twice per revolution [26].

**Localized outer race fault (ideal):** the peak frequencies in the envelope spectrum of the vibration signal generated by an outer race fault are the BPFO and its harmonics, ideally not modulated by the shaft rotational frequency, i.e. no sidebands around the BPFO [4].

**Localized inner race fault (ideal):** including the BPFI and its harmonics, the peak frequencies in the envelope spectrum of the vibration signal generated by an inner race fault also include  $1\times$ , its harmonics, and  $1\times$  or higher order sidebands around the BPFI, since the signal is amplitude modulated with  $1\times$  as the fundamental frequency of the modulating signal [4].

**Localized outer race fault with imbalance/misalignment:** the peak frequencies in the envelope spectrum of the signal generated by an outer race fault with imbalance or misalignment include  $1\times$ , its low harmonics, BPFO, and BPFO harmonics [27].  $1\times$  sidebands might also appear in the envelope spectrum if the signal is amplitude modulated by the modulating signal with  $1\times$  being the fundamental frequency [28].

**Localized inner race fault with imbalance/misalignment:** the peak frequencies in the envelope spectrum of the signal generated by an outer race fault with imbalance or misalignment include  $1\times$ , its low harmonics, BPFI and BPFI harmonics with  $1\times$  or higher order sidebands [1].

**Any fault with a gearbox:** the peak frequencies in the frequency/envelope spectrum of the signal generated by any bearing fault with the interference signal transmitted from gears can be dominated by the gear meshing frequency and its harmonics [16].

From **Table 1**, there are many observations useful for the estimation of the ISRF (i.e.  $1\times$ ) listed as follows:

- (1) Interference signals such as the gear meshing signal should be removed for bearing fault diagnosis;
- (2) Frequency component  $1\times$  is generally included in the original vibration signal due to unbalance or misalignment and appears to be the component with the lowest frequency;
- (3) Frequency component  $1\times$  may not be included in the perfectly processed signal if the bearing fault is an outer race fault;
- (4) If (3) happens, based on (2), the frequency component  $1\times$  should be included in the signal removed from the original signal.

These observations imply that the interference has to be removed before estimating the shaft rotational frequency. Additionally, the shaft rotational frequency can be estimated as the lowest peak frequency in the envelope frequency of the interference-free signal. However, it is possible that the shaft

**Table 1**  
Peak frequencies in frequency or envelope spectra of the signal generated in different situations.

No.	Faults	Peak frequencies in frequency spectrum	Peak frequencies in envelope spectrum
1	Unbalance (imbalance)	$1\times, 2\times, 3\times\dots$	–
2	Misalignment	$1\times, 2\times, 3\times\dots$ or $2\times, 4\times\dots$ under some conditions	–
3	Localized outer race fault	–	BPFO and BPFO harmonics
4	Localized inner race fault	–	$1\times, 1\times$ low harmonics, BPFI and BPFI harmonics with $1\times$ sidebands
5	Localized outer race fault with imbalance/misalignment	–	$1\times, 1\times$ low harmonics, BPFO and harmonics (with $1\times$ sidebands under some conditions)
6	Localized inner race fault with imbalance/misalignment	–	$1\times, 1\times$ low harmonics, BPFI and harmonics with $1\times$ sidebands
7	Any fault with gearboxes	Gear meshing frequency and its harmonics	Gear meshing frequency and its harmonics

rotational frequency does not appear in the envelope signal if the unbalance/misalignment signal is removed when the bearing has an outer race fault. Since the machinery cannot be operated under ideal conditions (no unbalance or misalignment), the shaft rotational frequency is normally present in the frequency spectrum of the collected vibration signal. In view of this, if the shaft rotational frequency does not appear in the envelope spectrum, then it is possible to find it in the frequency spectrum of the removed interference signal. Therefore, the removed interference signal should also be used to estimate the ISRF for bearing fault diagnosis under time-varying speed conditions.

## 2.2. Oscillatory features of bearing vibration signal

As mentioned above, the bearing fault-induced signal is composed of impulse responses caused by the bearing local defect, which can be considered to be low oscillatory due to the impulsiveness [25]. Compared to the bearing fault-induced signal, an interference signal such as one due to gear meshing is less spiky, which can be considered as high oscillatory. In this section, the bearing fault-induced signal and the interference signal are simulated via signal models to demonstrate their oscillatory behaviors under time-varying speed conditions.

A bearing fault-induced signal can be simulated as a series of impulse responses which occur at the FCF along the time span of the signal [16]. For a bearing operating under time-varying speed conditions, the equation for a signal model is given as [15]

$$\begin{aligned} x_B(t) &= [1 + A(t)] \sum_{m=1}^M s_m(t) \\ &= [1 + \alpha \cos(2\pi f_r t)] \sum_{m=1}^M L_m e^{-\beta(t-t_m)} \sin[\omega_r(t-t_m) + \phi_m] u(t-t_m) \end{aligned} \quad (3)$$

where  $A(t) = \alpha \cos(2\pi f_r t)$  represents the modulated waveform of frequency  $f_r$ ,  $\alpha$  is the amplitude of the modulation ( $\alpha < 1$ ),  $M$  is the number of impulse responses which is determined by the signal length  $T$  and the FCF,  $s_m(t)$  represents the  $m$ th impulse response,  $L_m$  is the amplitude of the  $m$ th impulse response,  $\beta$  is the coefficient related to damping,  $\omega_r$  is the excited resonance frequency or damped frequency of the vibration system,  $\phi_m$  is the phase of the  $m$ th impulse response, and  $u(t)$  is the unit step function. In the previous equation,  $t_m$  is the occurrence time of the  $m$ th impulse response which is calculated as

$$\begin{cases} t_1 = (1 + \delta_1)[1/f_c(0)] \\ t_m = (1 + \delta_m)[1/f_c(0) + 1/f_c(t_1) + \dots + 1/f_c(t_{m-1})] \end{cases} \quad m = 2, 3, \dots, M \quad (4)$$

where  $\delta_m$  is the random slippage ratio which on average varies between 0.01 and 0.02 [4],  $f_c(t)$  denotes the IFCF calculated by the Fault Characteristic Coefficient (FCC) and rotational frequency with  $f_c(t) = \text{FCC} * f_r(t)$ , and the time interval between the  $(m-1)$ th impulse response and the  $m$ th impulse response is  $(1+\delta)/f_c(t_{m-1})$ .

One set of interferences can be simulated as the sum of sinusoidal functions at the frequency of the interference and its harmonics, given as [15]

$$I(t) = \sum_{n_i=1}^{N_i} B_{n_i} \sin(2\pi n_i f_i t) \quad (5)$$

where  $N_i$  is the number of sinusoidal functions,  $B_{n_i}$  is the amplitude, and  $f_i$  is the time-varying frequency of the interference, referred to as the Instantaneous Interference Frequency (IIF) in this paper. The interference contained in the signal can be possibly more than one

set. It is indicated in [18] that the vibration signal also comprises the interference with the ISRF as the fundamental frequency caused by misalignment, eccentricity or imbalance. Therefore, the interference signal can be simulated as

$$x_I(t) = I_1(t) + I_2(t) = \sum_{n_{1i}=1}^{N_1} B_{1n_i} \sin(2\pi n_{1i} f_i t) + \sum_{n_{2i}=1}^{N_2} B_{2n_i} \sin(2\pi n_{2i} f_i t) \quad (6)$$

Examples of a simulated bearing fault-induced signal and interference signal are shown in Fig. 1(a) and (b), respectively. The bearing fault-induced signal is simulated by Eq. (3) with  $f_r = 20 t + 10$  Hz,  $\alpha = 0.95$ ,  $L_m = 1$ ,  $\beta = 1500$ ,  $\omega_r = 4000 * 2\pi$  rad/s,  $\phi_m = 0$ ,  $\delta_m$  is a random number with a mean of 0.01, FCC = 3.7, and  $T = 1$  s which gives  $M = 74$ . The interference is simulated by Eq. (6) with  $N_1 = 3$ ,  $f_i = 50 t + 20$  Hz,  $B_1 = [1, 0.3, 0.1]$ , and  $I_2(t) = 0$ . As shown in Fig. 1(a), the bearing fault-induced signal is composed of impulse responses which die out with an exponential decay; this can be considered as low oscillatory behavior. Also, the maximum amplitudes of the impulse responses are varied in proportion to the waveform  $A(t)$  since the signal is amplitude modulated with  $A(t)$  as the modulation waveform. The interval between two responses is the reciprocal of the IFCF. It can be seen that the interval becomes smaller with an increase in the shaft rotational frequency  $f_r$ . Compared to the bearing fault-induced signal, the interference signal shown in Fig. 1(b) is smoother since the signal is continuously oscillating. Therefore, the interference can be considered as high oscillatory behavior. It can be seen that even if the frequencies are time-varying, the bearing fault-induced signal and the interference signal can still be regarded as low oscillatory and high oscillatory, respectively. The variation in time of the rotational speed affects frequencies but does not affect the characteristic signal behavior of each component; hence, this can be exploited for signal decomposition. As a consequence, an approach to signal decomposition based on signal behavior (rather than frequency) such as the OBSD should be able to separate the bearing fault signature as the low oscillatory component and interference as the high oscillatory component from a contaminated signal, even under time-varying speed conditions.

## 3. Proposed method for bearing fault diagnosis under time-varying speed conditions

Based on the analysis in Section 2, a method is proposed for bearing fault diagnosis under time-varying speed conditions without signal resampling and without using tachometers. The flowchart of the proposed method is shown in Fig. 2. The proposed method consists of 3 main steps.

Step 1, the OBSD method is applied to the raw signal which is contaminated by interferences and noise. Using the OBSD, the raw signal is decomposed into a low oscillatory component, a high oscillatory component and the residual. The low oscillatory component is taken as the bearing fault signature and the high oscillatory component is taken as the interference due to the oscillatory features demonstrated in Section 2.2.

Step 2, an IFCF&ISRF search algorithm is proposed to estimate the IFCF and ISRF from the TFR of the result of step 1. The TFR is obtained via either the STFT (high oscillatory component) or Hilbert Transform and STFT (low oscillatory component). The IFCF and ISRF are extracted from the TFR and estimated by the frequency features analyzed in Section 2.1.

Step 3, bearing faults are identified via matching the curve-to-curve Average Ratio (AR) of the estimated IFCF and ISRF (step 2) to the FCC.

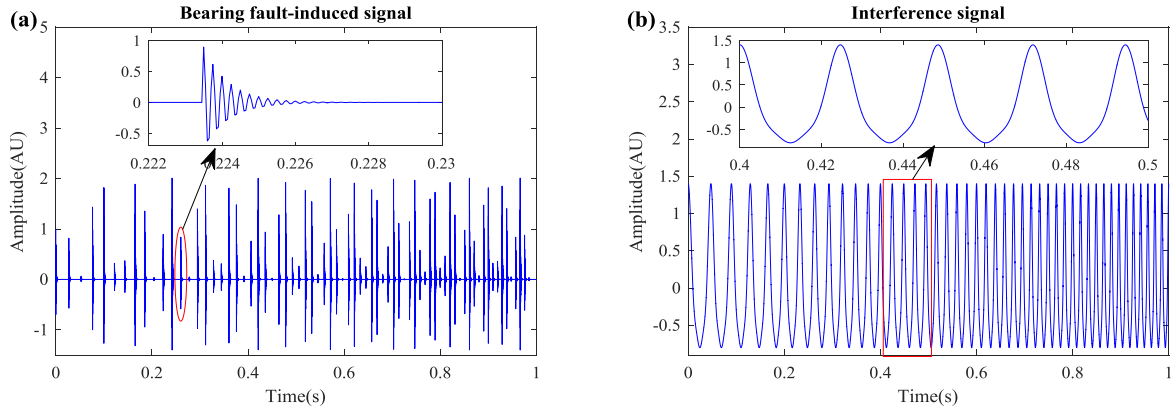


**Fig. 1.** Examples of the simulated bearing fault-induced signal and the interference signal. (a) Simulated bearing fault-induced signal, and (b) simulated interference signal.

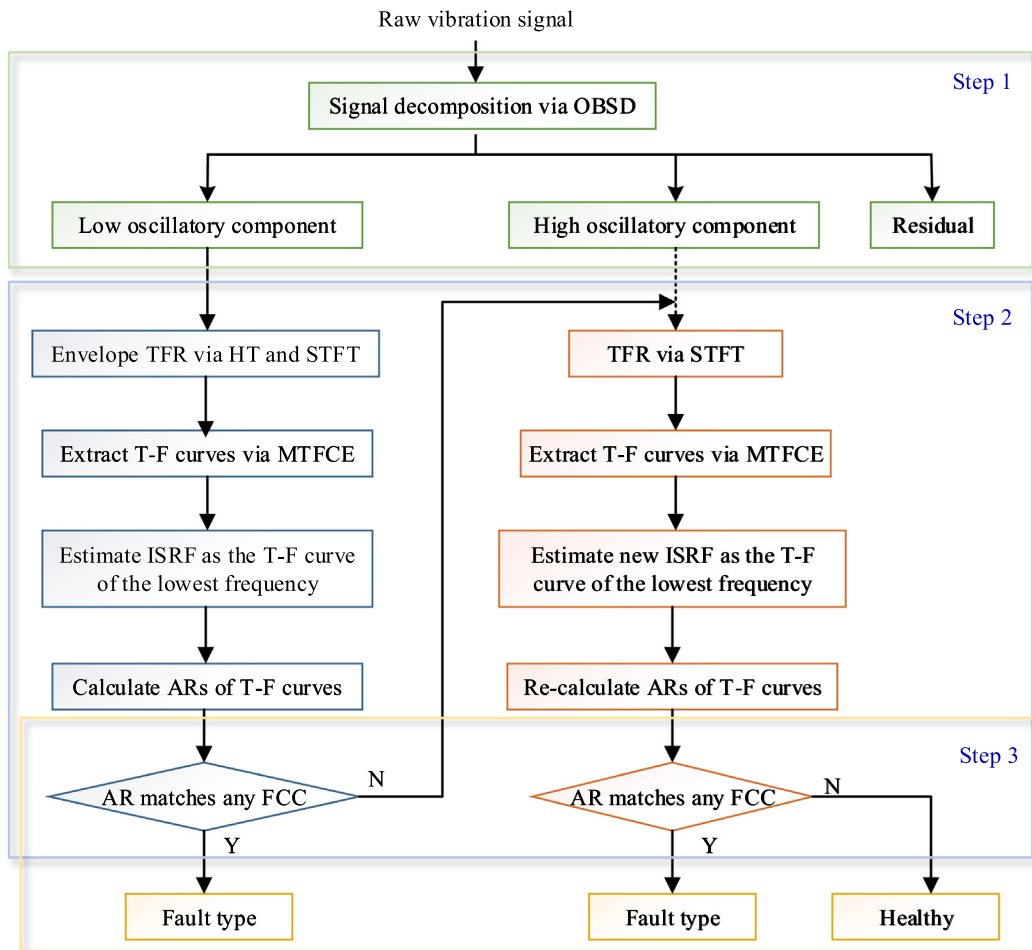


**Fig. 2.** Flowchart of the proposed bearing fault diagnosis method under time-varying speed conditions.

The flowchart of the proposed method is shown in Fig. 2. The details of each step are explained in each of the following subsections.

### 3.1. Bearing fault signature extraction via OBSO under time-varying speed conditions

The essence of the OBSO method is using two set of wavelets with different oscillatory behaviors to estimate a given signal [22]. The signal is decomposed into a low oscillatory component

and a high oscillatory component by the OBSO. According to the features of the bearing fault-induced signal and the interference signal, the bearing fault-induced signal is more impulsive which can be considered as low oscillatory behavior, and the interference is smoother which can be considered as high oscillatory behavior [23]. Therefore, the OBSO method can be used to extract the bearing fault signature from a signal obscured by interferences.

Compared to frequency or scale based methods for interference removal, the OBSO is superior since the signal decomposition is based on oscillatory behavior rather than frequencies. A Q-factor,

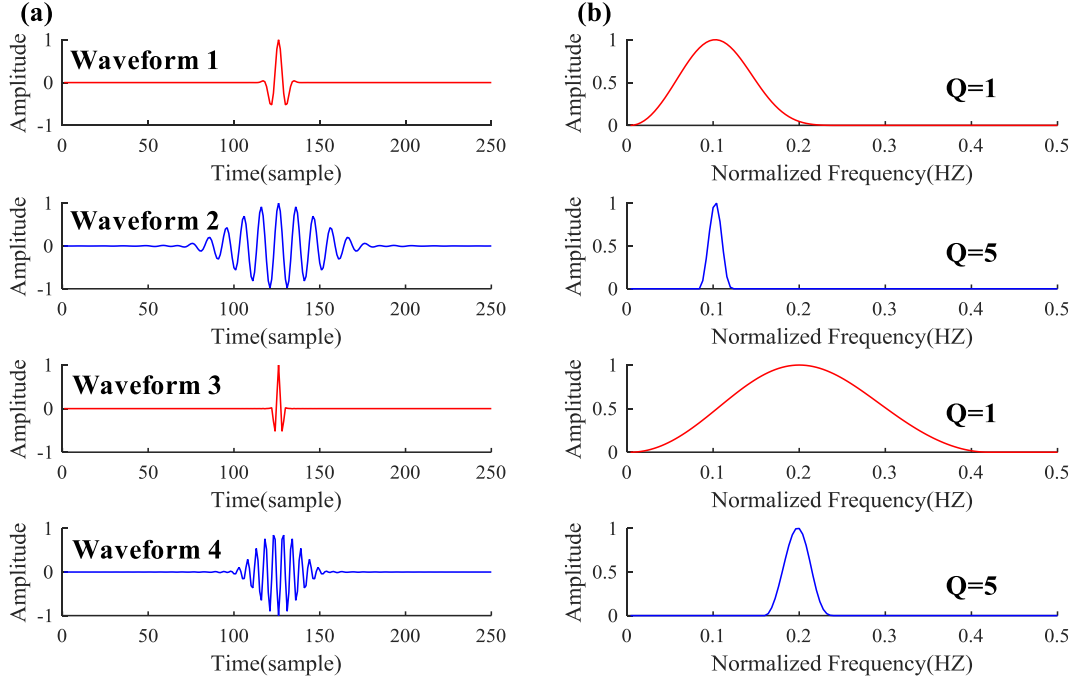


**Fig. 3.** Wavelets and their frequency spectra (cited from [29] with minor changes).

defined as the ratio of the center frequency to the bandwidth of the frequency response, is used to describe the oscillatory behavior of a wavelet [29]. A higher value of the Q-factor indicates a higher level of oscillation. In Fig. 3, four wavelets and their frequency spectra are shown. The Q-factors of the waveforms are also given. It can be seen that waveform 1 and waveform 2 have different oscillatory behaviors. However, their frequency spectra share the same center frequency. The same can be observed for waveform 3 and waveform 4. Under such circumstances, frequency-based band-pass filters would not be able to separate waveforms 1 and 2, nor waveforms 3 and 4. However, they can be separated according to their Q-factors. It is calculated that waveforms 1 and 3 have a Q-factor of 1 since they exhibit low oscillatory behavior, and waveforms 2 and 4 have a Q-factor of 5 since they have relatively high oscillatory behavior. Additionally, this demonstrates that waveforms that have the same oscillatory behavior have the same the Q-factors, even if the center frequencies are different. This makes the OBSD effective for capturing the true features that are useful for bearing fault signature extraction under time-varying speed conditions.

The OBSD method employs the Tunable Q-factor Wavelet Transform (TQWT) and Morphological Component Analysis (MCA) to realize signal decomposition [22]. The TQWT is used to generate a set of wavelets that have the same Q-factor, i.e. the same oscillatory behavior. The wavelets can be obtained with the selection of three parameters,  $Q$  (Q-factor),  $r$  and  $P$ , where  $Q$  is related to the oscillatory behavior,  $r$  is related to the redundancy of the frequency responses, and  $P$  is the number of wavelets. By setting up two sets of wavelets, one set has low oscillatory behavior with parameters  $Q_l$ ,  $r_l$ , and  $P_l$ , and the other set has high oscillatory behavior with parameters  $Q_h$ ,  $r_h$ , and  $P_h$ , the signal decomposition can be completed by MCA. The wavelet coefficients are obtained via optimization [22] as

$$\begin{bmatrix} \mathbf{w}_h^{opt} \\ \mathbf{w}_l^{opt} \end{bmatrix} = \underset{\mathbf{w}_l, \mathbf{w}_h}{\operatorname{argmin}} \| \mathbf{y} - \mathbf{S}_l \mathbf{w}_l - \mathbf{S}_h \mathbf{w}_h \|_2^2 + \lambda_l \| \mathbf{w}_l \|_1 + \lambda_h \| \mathbf{w}_h \|_1 \quad (7)$$

where  $\mathbf{w}_l$  refers to wavelet coefficients for the low oscillatory component,  $\mathbf{w}_h$  stands for the wavelet coefficients for the high oscillatory component,  $\mathbf{w}_l^{opt}$  and  $\mathbf{w}_h^{opt}$  are results after the optimization,  $\mathbf{y}$  is the signal to be decomposed,  $\mathbf{S}_l$  refers to wavelets obtained via the TQWT for the low oscillatory component,  $\mathbf{S}_h$  represents wavelets for the high oscillatory component,  $\lambda_l$  is the regularization parameter for the low oscillatory component,  $\lambda_h$  is the regularization parameter for the high oscillatory component,  $\| \cdot \|_1$  and  $\| \cdot \|_2$  are the norm-1 and norm-2 operations, respectively. This optimization problem can be solved using an iterative algorithm called Split Augmented Lagrangian Shrinkage Algorithm (SALSA), obtained as [22]

$$\mathbf{w}_i^k = f(\mathbf{w}_i^{k-1}, \mu), i = l, h, k = 1, 2, \dots, K \quad (8)$$

where  $\mu$  is the penalty parameter and  $K$  is the maximum number of iterations. Details of the solution can be found in the appendix in [25]. With the calculated wavelet coefficients, the decomposed low oscillatory and high oscillatory components can then be obtained by inverse TQWT with the optimized wavelet coefficients.

A guidance for the selection of the parameters when applying the OBSD to bearing fault signature extraction under constant speed is given in [25]. Since the OBSD method is frequency independent, the same approach can be used for the selection of OBSD parameters under time-varying speed conditions.

### 3.2. IFCF & ISRF search algorithm

The IFCF and ISRF can be estimated from the envelope TFR or TFR of the decomposed signal obtained via the OBSD. The T-F curves in the TFR can be extracted via the multiple time-frequency curve extraction (MTFCE) algorithm [30]. However, the ISRF may appear in either/both the low oscillatory or/and high oscillatory components produced by the OBSD according to the analysis in Section 2. Hence, the ISRF cannot be simply estimated from the decomposed low oscillatory component. To address this issue, an IFCF&ISRF search ISRF search algorithm is proposed and the flowchart of the algorithm is step 2 shown in Fig. 2.

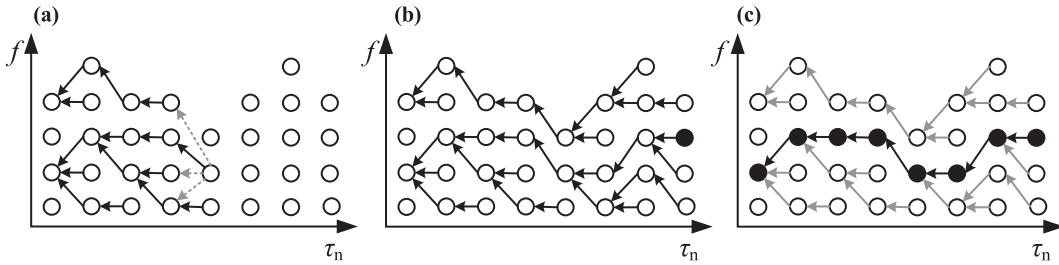


Fig. 4. Scheme of T-F curve extraction from the TFR.

### 3.2.1. MTFCe

An algorithm for multiple T-F curve extraction was proposed for bearing fault diagnosis under time-varying speed conditions in [30]. With this algorithm, multiple T-F curves can be extracted from the TFR of a signal. The algorithm iteratively utilizes fast path optimization for T-F curve extraction.

Fast path optimization for T-F curve extraction from the TFR is achieved by optimally extracting a string of peaks along the time span [31]. A scheme of the T-F curve extraction is shown in Fig. 4. The circles in the TFR represent peaks at moment  $\tau_n$ . Each peak at  $\tau_n$  links one peak at the past moment  $\tau_{n-1}$ . The linked peak at  $\tau_{n-1}$  can be determined by optimization with a cost function. After every peak links to one of the peaks at the previous moment, many paths are generated in the peak map, as shown in Fig. 4(b). Finally, by selecting the point of the minimum value of the cost function at the last moment, the whole T-F curve can be extracted following the path as shown in Fig. 4(c). Compared to T-F curve extraction methods by searching local maxima, the fast path optimization method can effectively prevent unexpected frequency jumps in the extracted T-F curve [31].

The multiple T-F curve extraction algorithm is developed by iteratively utilizing the fast path optimization method. The procedure of the algorithm is as follows:

- Step 1. Extract one T-F curve from the TFR using the fast path optimization method;
- Step 2. Remove the peaks of the last extracted T-F curve from the peak map and generate a new peak map;
- Step 3. Extract a new T-F curve from the new peak map via the fast path optimization method;
- Step 4. Repeat steps 2 and 3 to extract a new T-F curve until the number of extracted curves reaches the preset maximum number  $C_{\max}$ .

The maximum number of extracted T-F curves should ensure that enough curves are extracted from the TFR. However, the computational cost increases with the increase of the number of extracted curves. Therefore,  $C_{\max}$  should be selected as large enough within the acceptable computational cost. In this paper,  $C_{\max}$  is set as 4 in Sections 4 and 5.

### 3.2.2. True IFCF&ISRF search

It is supposed that the low oscillatory component obtained via the OBSD is the extracted bearing fault signature. If the bearing is faulty, then the IFCF and its harmonics should show peaks in the envelope TFR of the low oscillatory component. In addition, the ISRF may also appear in the envelope TFR of the extracted bearing fault signature and it is the T-F curve of the lowest frequency. Thus, the T-F curve of the lowest frequency is regarded as the ISRF. Then, the AR of each curve to the estimated ISRF is calculated. The AR is defined as

$$R_a = \frac{1}{N} \sum_{n=1}^N \frac{f_p(\tau_n)_i}{f_p(\tau_n)_l} \quad (9)$$

where  $N$  is the length of the extracted curves,  $f_p(\tau_n)_l$  denotes the bottom T-F curve, i.e. the T-F curve with the lowest frequency, and  $f_p(\tau_n)_i$  is one of the extracted T-F curves. According to the frequency features discussed in section 2.1, the IFCF is proportional to the ISRF and the ratio IFCF/ISRF is the FCC. The calculated curve-to-curve AR may not exactly match the FCC due to the limited resolution of the TFR obtained via the STFT. Therefore, a 5% relative error of the calculated average ratio to the FCC is proposed for the tolerance of matching. If the calculated AR matches the FCC of any type fault, then the corresponding T-F curve is estimated as the IFCF.

However, the ISRF may not be included in the envelope TFR of the extracted bearing fault signature. As mentioned in Section 2, if the ISRF is not found in the extracted bearing fault signature, then the ISRF should appear in the TFR of the high oscillatory component obtained via the OBSD. Therefore, if all the AR calculated from the low oscillatory component do not match any of the FCC, then the TFR of the high oscillatory component is also utilized to estimate the ISRF. Similarly, the extracted T-F curve of the lowest frequency is estimated as the ISRF. The AR of each T-F curve extracted from the envelope TFR of the low oscillatory component to the new estimated ISRF is re-calculated. If the AR matches the FCC of any fault type, then the corresponding T-F curve is considered as the IFCF. Otherwise, no IFCF is estimated from the result of the decomposed signal.

### 3.3. Fault identification via AR and FCC

It is known that the FCF for each fault type is proportional to the shaft rotational speed and the ratio of the FCF to the rotational frequency is constant [4]. In this paper, this ratio is called the Fault Characteristic Coefficient (FCC). For bearings with outer race fault or inner race fault, the FCF and FCC can be calculated by

$$FCC_O = BPFO/f_r = \frac{n_b}{2} \left( 1 - \frac{d}{D} \cos\phi \right) \quad (10)$$

$$FCC_I = BPFI/f_r = \frac{n_b}{2} \left( 1 + \frac{d}{D} \cos\phi \right) \quad (11)$$

where  $n_b$  is the number of rolling elements,  $d$  is the diameter of the rolling element,  $D$  is the pitch diameter of the bearing,  $\phi$  is the angle of the load from the radial plane,  $f_r$  is the shaft rotational frequency,  $FCC_O$  and  $FCC_I$  are the outer race FCC and inner race FCC, respectively. Since the FCC is independent of the shaft rotational frequency, bearing faults can still be diagnosed by the FCC under time-varying rotational speed conditions. Therefore, if both the IFCF and the ISRF are extracted, the fault can be diagnosed by matching the average ratio of IFCF/ISRF to the FCC.

With the estimated IFCF and ISRF via the IFCF&ISRF search algorithm, the bearing fault can be diagnosed by matching the calculated AR to the FCC. If there is no IFCF estimated via the IFCF&ISRF search algorithm, then the bearing is considered to be healthy.

#### 4. Simulations

To investigate the effectiveness of the proposed method for bearing fault diagnosis under time-varying speed conditions, simulations are conducted. The signal is simulated as a mixture of a bearing fault-induced signal, interferences and random noise:

$$x(t) = x_B(t) + x_I(t) + n(t) \quad (12)$$

where  $n(t)$  represents random noise with intensity measured by its Signal-to-Noise Ratio (SNR).

##### 4.1. Cases when IFCF and IIF do not cross

The simulation starts with a simulated signal in which the IFCF does not cross the IIF, i.e. the IFCF and the IIF are proportional to each other. To test the effectiveness of the OBSO for bearing fault signature extraction, the IFCF and the IIF are chosen to be very close.

###### 4.1.1. Case 1: ISRF is not modulated by the bearing fault-induced signal

In this simulation, the raw signal is composed of a bearing fault-induced signal, interference signal, and random noise. To simulate the signal of a faulty bearing with an outer race fault, the bearing fault-induced signal is not amplitude-modulated with the ISRF as the frequency of the modulation signal. The raw signal is simulated by Eq. (12) with  $f_r = 20 t + 3$  Hz,  $\alpha = 0$ ,  $L_m = 1$ ,  $\beta = 500$ ,  $\omega_r = 4000^*2\pi$  rad/s,  $\phi_m = 0$ ,  $\delta_m$  is a random number with a mean of 0.01, FCC = 3.7,  $T = 5$  s,  $N_1 = 3$ ,  $f_I = 4f_r$ ,  $B_1 = [1.5, 1, 0.25]$ ,  $N_2 = 2$ ,  $B_2 = [0.5, 0.25]$ , and SNR = -5 dB. The sampling rate is 20 kHz and the sampling time is 5 s. The simulated raw signal is shown in Fig. 5(a). The envelope TFR of the simulated “pure” bearing fault induced signal and the TFR of the simulated interference signal are shown in Fig. 5(b) and (c), respectively. From Fig. 5(b), the IFCF and its harmonics can be observed. From Fig. 5(c), the IIF, the ISRF, and their harmonics can be observed. Additionally, the envelope TFR of the

raw signal is shown in Fig. 5(d), which is obtained by applying the Hilbert transform and the STFT to the raw signal. The IIF is dominant in the TFR in Fig. 5(d). Also, the ISRF can be observed even though it is not very clear. However, it is difficult to discern the IFCF from the IIF since IFCF = 3.7  $f_r$  is so close to IIF which is 4  $f_r$ . Obviously, it is impossible to detect the fault accurately directly from the raw signal.

The signal is then decomposed into a low oscillatory component, a high oscillatory component, and the residual via the OBSO, according to the proposed method. The parameters related to OBSO are chosen as  $Q_l = 1$ ,  $r_l = 6$ ,  $P_l = 51$ ,  $Q_h = 9$ ,  $r_h = 6$ ,  $P_h = 230$ ,  $\lambda_l = \lambda_h = 0.8$ ,  $\mu = 2$ , and  $K = 200$ . The low oscillatory component and the high oscillatory component are shown in Fig. 6(a) and (b), respectively. The decomposed low oscillatory component is taken as the extracted bearing fault signature. The envelope TFR of the low oscillatory component is shown in Fig. 6(c). It can be seen that only the IFCF and its harmonics appear in the TFR, while the IIF, ISRF, and their harmonics disappear which implies the interference is completely removed. The TFR of the high oscillatory component is shown in Fig. 6(d). Only the IIF, the ISRF, and their harmonics show ridges in the TFR, the same as the TFR in Fig. 5(c), which also implies that the signal is effectively decomposed. Subsequently, the multiple T-F curve extraction algorithm is applied to the envelope TFR of the low oscillatory component and the four extracted curves are shown in Fig. 6(e). In addition, the average ratios are calculated as 1, 2, 3, and 4, respectively. None of the average ratios match the given FCC (3.7) within a 5% relative error. The reason for this is that the ISRF does not appear in the TFR shown in Fig. 6(c). Therefore, following the proposed ISRF-search fault diagnosis strategy, the multiple T-F curve extraction algorithm is applied to the TFR of the high oscillatory component and the four newly extracted curves are shown in Fig. 6(f). The extracted T-F curves are the ISRF and its 2nd harmonic, and the IIF and its 2nd harmonic. A new T-F curve figure is shown in Fig. 6(g), which is composed of four curves in Fig. 6(e) and the curve of the lowest frequency in Fig. 6(f). By taking the newly added curve in Fig. 6(g) as the bottom curve for the re-calculation of the average ratios, the average ratios for the four other curves in Fig. 6(f) are recalculated as 3.70, 7.40, 11.11, and 14.80. Among these average ratios, 3.70 matches the given FCC (3.7) and the three other ratios match the 2nd, the 3rd, and the 4th harmonics, respectively. Thus,

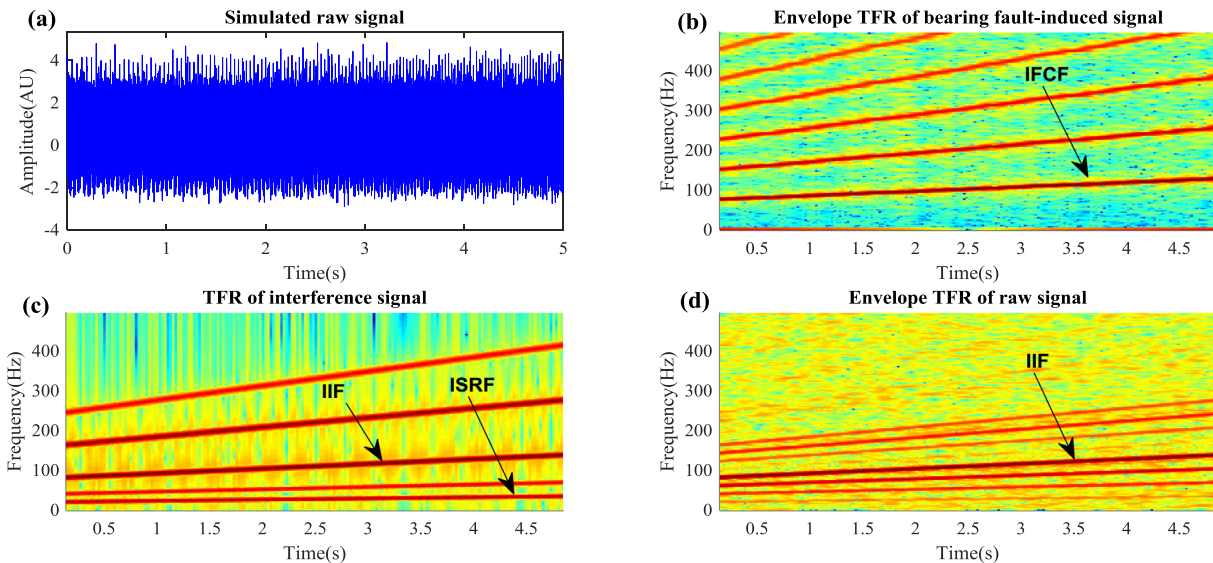


**Fig. 5.** Simulated signal for case 1. (a) Simulated raw signal, (b) envelope TFR of the bearing fault-induced signal, (c) TFR of the interference signal, and (d) envelope TFR of the raw signal.

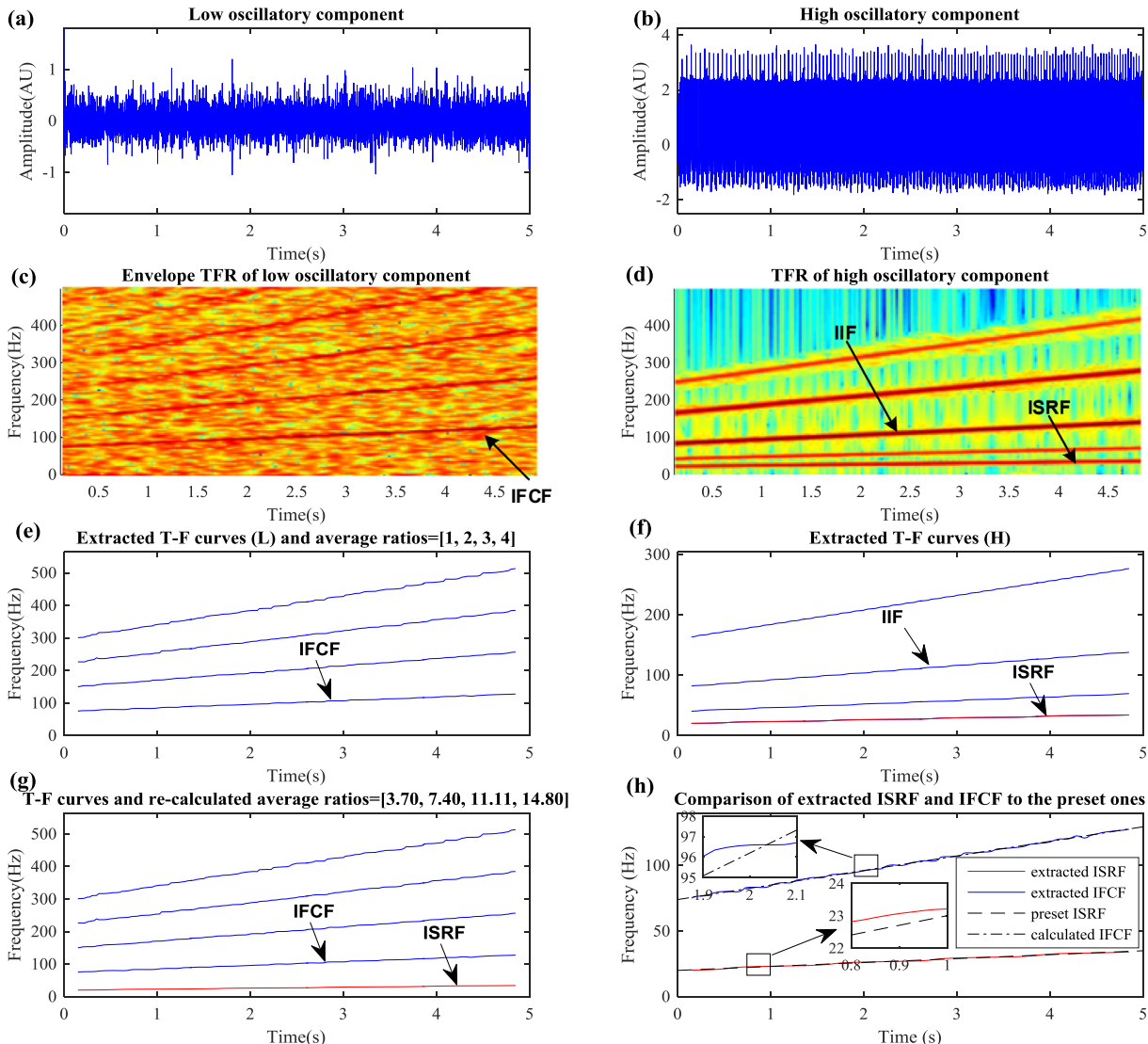


**Fig. 6.** Results of simulation case 1 via the proposed method. (a) Decomposed low oscillatory component via OBSD, (b) decomposed high oscillatory component, (c) envelope TFR of low oscillatory component, (d) TFR of high oscillatory component, (e) extracted T-F curves from (c), (f) extracted T-F curves from (d), (g) T-F curves used for bearing fault diagnosis, and (h) comparison of extracted ISRF and IFCF to the preset ones.

the bearing is diagnosed as faulty via the proposed method. Additionally, the new bottom curve in Fig. 6(g) is considered as the extracted ISRF and the curve with the second lowest frequency is considered as the extracted IFCF.

To compare the extracted ISRF to the preset ISRF and the extracted IFCF to the preset IFCF, a comparison figure is shown in Fig. 6(h). The average relative error of the extracted IFCF to the present IFCF is calculated as 0.36% and the average relative error of the extracted ISRF to the preset ISRF is calculated as 1.21%. It can be seen that both the extracted ISRF and the extracted IFCF fit the preset curves which further confirms the effectiveness of the proposed method.

#### 4.1.2. Case 2: ISRF is modulated by the bearing fault-induced signal

To further test the performance of the proposed fault diagnosis strategy, some changes were made to the simulated signal in case 1. In this simulation, the bearing fault-induced signal is amplitude modulated with the ISRF as the frequency of the modulation signal, i.e., the ISRF will appear in the envelope TFR of bearing fault-induced signal, which is similar to the case of bearing signal with

inner race fault. The original signal is simulated by Eq. (12) with  $f_r = 20 t + 3$  Hz,  $\alpha = 0.95$ ,  $L_m = 1$ ,  $\beta = 500$ ,  $\omega_r = 4000 \times 2\pi$  rad/s,  $\phi_m = 0$ ,  $\delta_m$  is random number with a mean of 0.01, FCC = 3.7,  $T = 5$  s,  $f_i = 4 f_r$ ,  $N_1 = 3$ ,  $B_1 = [1.5, 1, 0.25]$ ,  $N_2 = 2$ ,  $B_2 = [0.5, 0.25]$ , and SNR = -5 dB. The sampling rate is 20 kHz and the sampling time is 5 s. The only difference from the simulation in case 1 is that  $\alpha$  is changed from 0 to 0.95. The simulated raw signal is shown in Fig. 7(a), which is a mixture of bearing fault-induced signal, two sets of interferences and noise. In addition, the envelope TFR of the raw signal is shown in Fig. 7(b), in which the IIF can be clearly observed. However, the IFCF cannot be observed in the envelope TFR which implies that the bearing fault cannot be detected and diagnosed without further analysis.

Applying the proposed method to the simulated raw signal, the decomposed low oscillatory component shown in Fig. 7(c), the high oscillatory component shown in Fig. 7(d) are obtained via the OBSD. Parameters related to the OBSD are selected as  $Q_l = 1$ ,  $r_l = 6$ ,  $P_l = 51$ ,  $Q_h = 7$ ,  $r_h = 6$ ,  $P_h = 189$ ,  $\lambda_l = \lambda_h = 0.7$ ,  $\mu = 2$ , and  $K = 250$ . The envelope TFR of the low oscillatory component is shown in Fig. 7(e) and the TFR of the high oscillatory component is

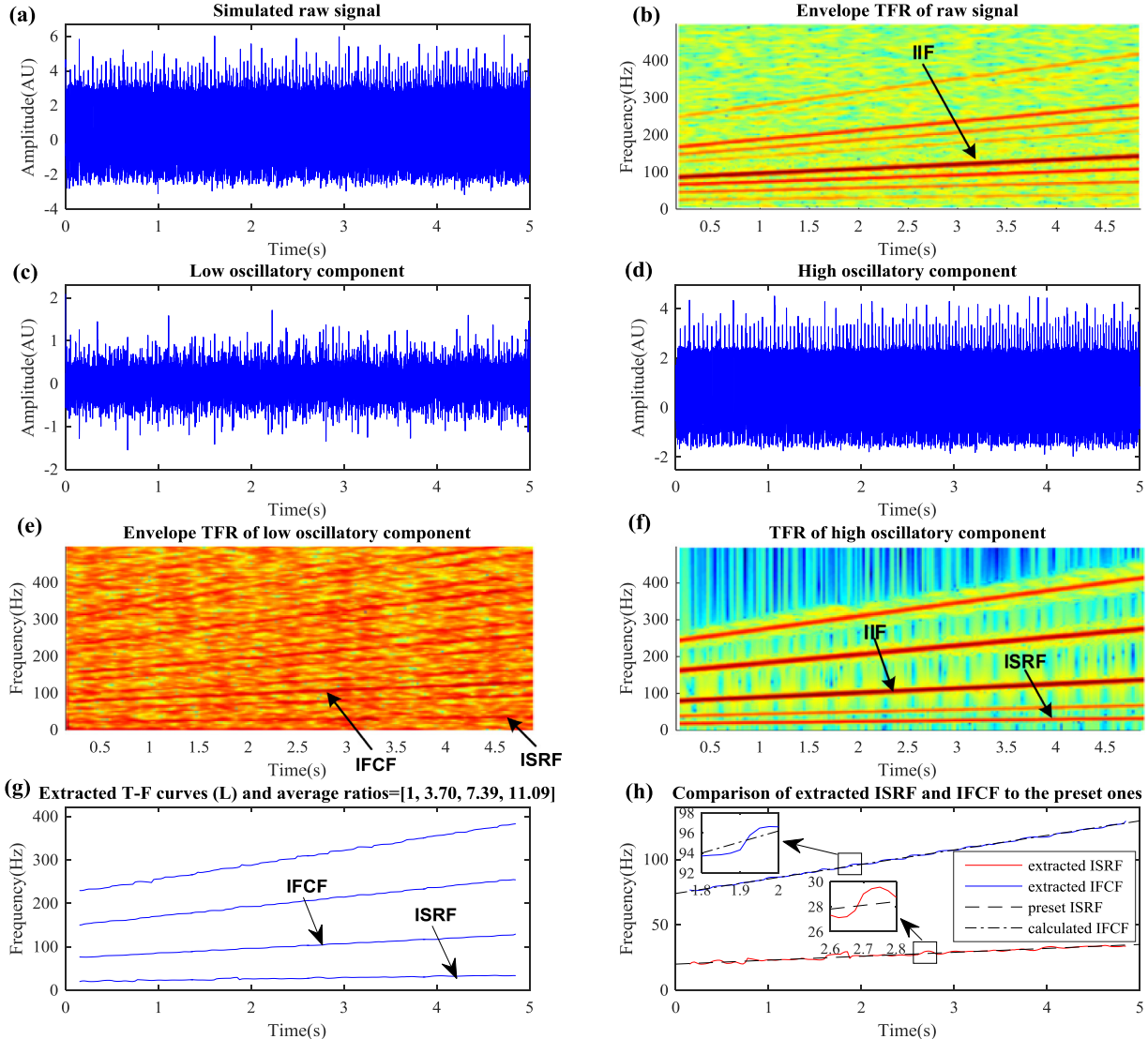


**Fig. 7.** Simulated signal and results for case 2. (a) Simulated raw signal, (b) envelope TFR of raw signal, (c) decomposed low oscillatory component via OBSD, (d) decomposed high oscillatory component, (e) envelope TFR of low oscillatory component, (f) TFR of high oscillatory component, (g) extracted T-F curves from (e), and (h) comparison of extracted ISRF and IFCF to their preset curves.

is shown in Fig. 7(f). The IFCF and its harmonics, the ISRF and sidebands can be observed in Fig. 7(e) without the presence of IIF and its harmonics, which implies that the bearing fault signature is effectively extracted from the contaminated raw signal via the OBSD. Additionally, the IIF and the ISRF, and their harmonics are clearly shown in Fig. 7(f), which also demonstrates that the signal is effectively separated. By applying the multiple T-F curve extraction algorithm to the envelope TFR shown in Fig. 7(e), four T-F curves are extracted as shown in Fig. 7(g). Taking the curve of the lowest frequency as the bottom curve, the average ratios for the 4 curves are calculated as 1, 3.70, 7.39, and 11.09, respectively. Among these average ratios, 3.70 matches exactly the given FCC (3.7). Additionally, 7.39 and 11.09 imply the 2nd and the 3rd harmonics of IFCF. Based on the result, the bearing fault can be diagnosed. Also, the bottom curve in Fig. 7(g) is considered as the extracted ISRF and the curve with the second lowest frequency is considered as the extracted IFCF.

A comparison figure, which includes the extracted ISRF, the present ISRF, the extracted IFCF, and the preset IFCF, is shown in Fig. 7(h). It can be observed that both the extracted ISRF and the

extracted IFCF fit the preset curves very well. The average relative error of the extracted IFCF to the preset IFCF is 0.46% and the average relative error of the extracted ISRF to the preset ISRF is 1.80%, which demonstrates the effectiveness of the proposed method.

#### 4.2. Cases when IFCF and IIF cross each other

To test the performance of the proposed method for different situations, two additional simulations are conducted in which the IFCF of the bearing fault-induced signal and the IIF of the interference cross each other. Theoretically, the OBSD should be able to separate the bearing signal from the interference in this situation since it is independent of frequency. This will be demonstrated in the following simulations.

##### 4.2.1. Case 3: linearly varying IFCF and IIF

In this simulation, the IFCF and IIF cross each other and both are linearly varying. Additionally, the ISRF is not modulated by the bearing fault-induced signal. Similarly, the interference signal is composed of two sets of interferences and one of them with ISRF

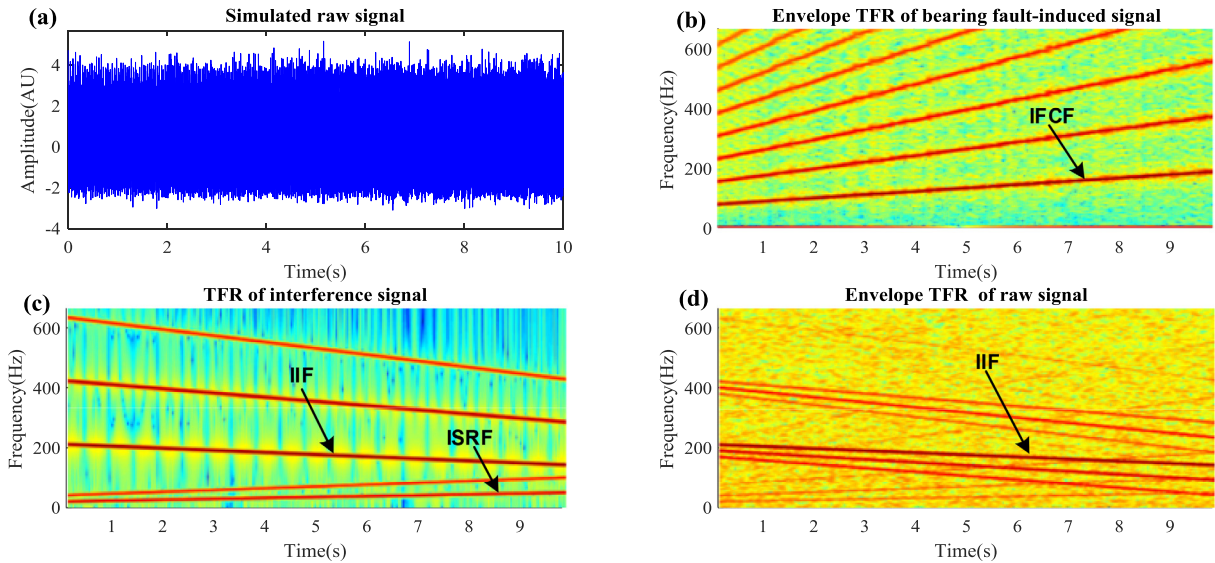


**Fig. 8.** Simulated signal for case 3. (a) Simulated raw signal, (b) envelope TFR of the bearing fault-induced signal, (c) TFR of the interference signal, and (d) envelope TFR of the raw signal.

as the fundamental frequency. The raw signal is simulated by Eq. (12) with  $f_r = 20t + 3$  Hz,  $\alpha = 0$ ,  $L_m = 1$ ,  $\beta = 500$ ,  $\omega_r = 4000 \cdot 2\pi$  rad/s,  $\phi_m = 0$ ,  $\delta_m$  is random number with a mean of 0.01, FCC = 3.7,  $T = 10$  s,  $N_1 = 3$ ,  $f_l = -7t + 210$ ,  $B_1 = [1.5, 1, 0.25]$ ,  $N_2 = 2$ ,  $B_2 = [0.5, 0.25]$  and SNR = -5 dB. The sampling rate is 20 kHz and the sampling time is 5 s. The simulated signal raw signal is shown in Fig. 8(a). The envelope TFR of the simulated bearing fault-induced signal is shown in Fig. 8(b), in which the IFCF and its harmonics can be observed. The TFR of the interference signal is shown in Fig. 8(c) which is dominated by the ridges of the interferences, i.e. the IIF and its two harmonics, and the ISRF and its 2nd harmonic. Moreover, the envelope TFR of the raw signal is shown in Fig. 8(d), in which the IFCF can barely be observed and it crosses the IIF. Again, the bearing fault cannot be detected directly without further investigation.

The OBSO is then applied to the raw signal to separate the bearing fault signature and interferences with parameters selected as  $Q_l = 1$ ,  $r_l = 6$ ,  $P_l = 51$ ,  $Q_h = 8$ ,  $r_h = 6$ ,  $P_h = 210$ ,  $\lambda_l = \lambda_h = 0.5$ ,  $\mu = 1$ , and  $K = 200$ . The decomposed low oscillatory component is shown in Fig. 9(a) and the high oscillatory component is shown in Fig. 9(b), respectively. The envelope TFR of the low oscillatory component is shown in Fig. 9(c) in which the IFCF and its harmonics can be clearly observed without the presence of the T-F curves of interferences. The TFR of the high oscillatory component is shown in Fig. 9(d) in which only the T-F curves of interferences can be seen, i.e. the IIF and its two harmonics, the ISRF and its 2nd harmonic. The results shown in Fig. 9(c) and (d) reveal that the bearing fault signature and the interference signal are effectively separated by the OBSO. According to the proposed method, the multiple T-F curve extraction algorithm is applied to the envelope TFR of the low oscillatory component and the extracted four curves are presented in Fig. 9(e). The average ratios are calculated as 1, 2, 3, and 4, respectively. Similar to the results in case 2, the extracted T-F curves are the IFCF and its harmonics. The bearing fault still cannot be diagnosed since none of the calculated average ratios match the given FCC (3.7). Therefore, according to the proposed ISRF-search diagnosis strategy, four extra T-F curves are extracted from the TFR of the high oscillatory component shown in Fig. 9(f) via the multiple T-F curve extraction algorithm. A new T-F figure is obtained as shown in Fig. 9(g) by adding the curve which has the lowest frequency in Fig. 9(f)–(e). The average ratios are recalculated as 3.7, 7.4, 11.1, and 14.8, respectively. Among these

average ratios, 3.7 matches the FCC and the rest of the ratios match the 2nd, 3rd, and 4th harmonic, respectively. Now the bearing fault can be successfully diagnosed. Additionally, the bottom curve and the curve with the second lowest frequency in Fig. 9(g) are considered as the extracted ISRF and the extracted IFCF, respectively.

To further examine the performance of the proposed method, the extracted ISRF, extracted IFCF, and their preset curves are plotted in Fig. 9(h). It can be seen that both the extracted ISRF and the extracted IFCF fit the preset curves quite well. The average relative error of the extracted IFCF to the preset IFCF is only 0.36% and the average relative error of the extracted ISRF to the preset ISRF is 0.93%. The comparison further testifies to the effectiveness of the proposed method.

#### 4.2.2. Case 4: linearly varying IFCF and non-linearly varying IIF

To further challenge the proposed method, non-linearly varying IIF of the interference is considered in this simulation while keeping linearly varying IFCF of the bearing fault-induced signal. Again, the IFCF and the IIF cross each other. Additionally, the bearing fault-induced signal is amplitude modulated with the ISRF as the frequency of the modulation signal. The raw signal is simulated by Eq. (12) with  $f_r = 20t + 3$  Hz,  $\alpha = 0.95$ ,  $L_m = 1$ ,  $\beta = 500$ ,  $\omega_r = 4000 \cdot 2\pi$  rad/s,  $\phi_m = 0$ ,  $\delta_m$  is a random number with a mean of 0.01, FCC = 3.7,  $T = 10$  s,  $N_1 = 3$ ,  $f_l = -6(t-5)^2 + 250$ ,  $B_1 = [1.5, 1, 0.25]$ ,  $N_2 = 2$ ,  $B_2 = [0.5, 0.25]$ , and SNR = -5 dB. The sampling rate is 20 kHz and the sampling time is 5 s. The simulated raw signal is shown in Fig. 10(a). The envelope TFR of the raw signal is shown in Fig. 10(b) in which the IFCF can only be vaguely observed, and the IFCF and the IIF cross each other. From the TFR in (b), the bearing fault once again cannot be diagnosed directly.

Therefore, the OBSO is applied to the raw signal. The low oscillatory component is shown in Fig. 10(c) and the high oscillatory component is shown in Fig. 10(d). Parameters related to the OBSO method are selected as  $Q_l = 1$ ,  $r_l = 6$ ,  $P_l = 51$ ,  $Q_h = 9$ ,  $r_h = 6$ ,  $P_h = 251$ ,  $\lambda_l = \lambda_h = 0.7$ ,  $\mu = 1$ , and  $K = 200$ . The envelope TFR of the low oscillatory component is shown in Fig. 10(e). The ISRF, the IFCF, and its harmonics can be observed in Fig. 10(e) without the appearance of the IIF. Also, the TFR of the high oscillatory component is shown in Fig. 10(f) in which only the IIF, the ISRF, and their harmonics appear. It indicates that the OBSO has effectively separated the bearing fault signature and the interference. Subsequently, the multiple T-F curve extraction algorithm is applied to the TFR

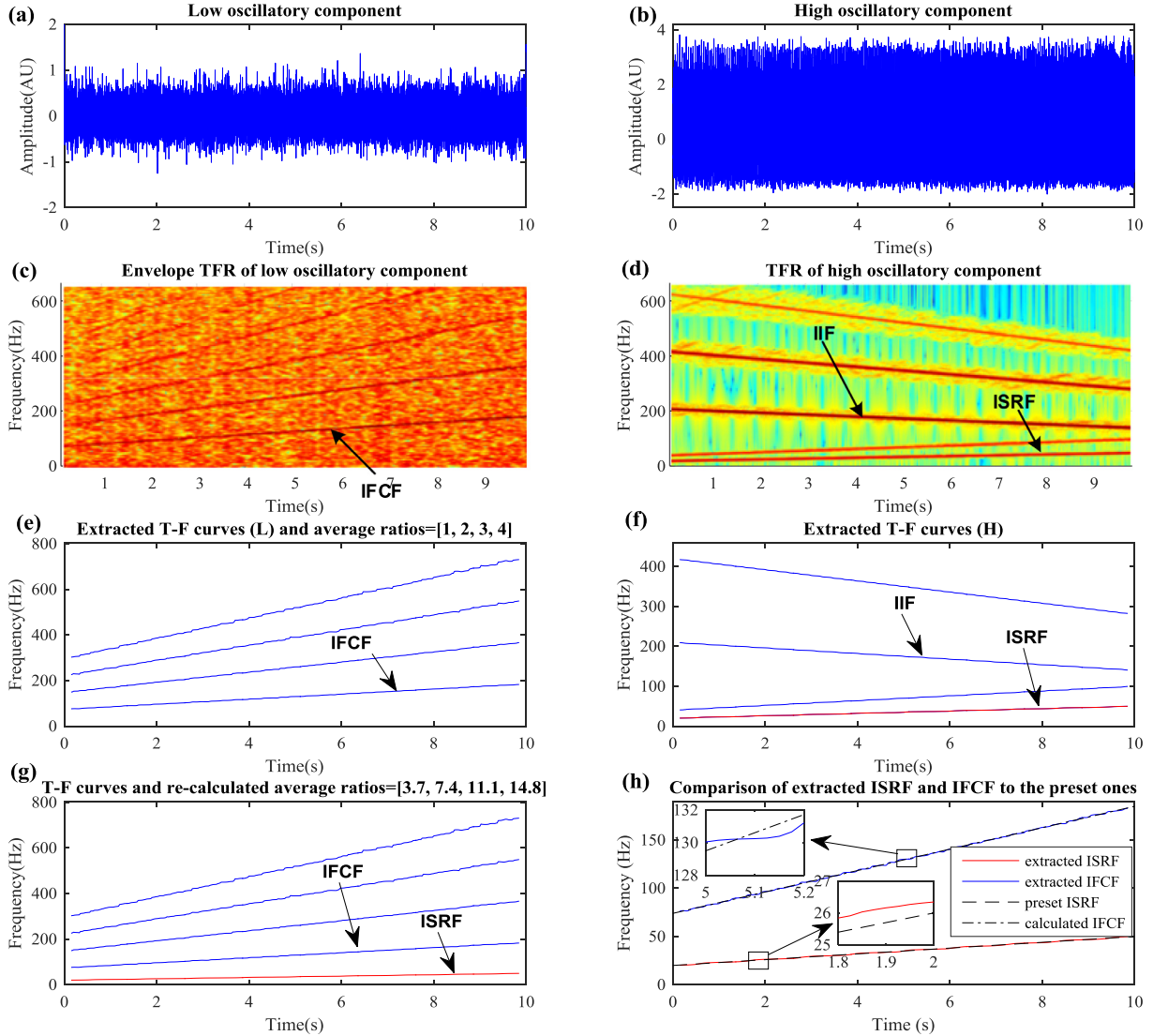


**Fig. 9.** Results of simulation case 3. (a) Decomposed low oscillatory component via OBSO, (b) decomposed high oscillatory component, (c) envelope TFR of low oscillatory component, (d) TFR of high oscillatory component, (e) extracted T-F curves from (c), (f) extracted T-F curves from (d), (g) T-F curves used for bearing fault diagnosis, and (h) comparison of extracted ISRF and IFCF to their preset curves.

shown in Fig. 10(e) and the extracted curves are shown in Fig. 10(g). The calculated average ratios are 1, 3.71, 7.42, and 11.13, respectively. Among these average ratios, 3.71 matches the FCC with very low relative error (0.27%). Additionally, 7.42 and 11.13 correspond to the 2nd harmonic and the 3rd harmonic, respectively. Thus, the bearing fault can be diagnosed via the proposed method. Furthermore, a comparison figure which includes the extracted ISRF, the preset ISRF, the extracted IFCF, and the preset IFCF is shown in Fig. 10(h). It can be seen that both the extracted IFCF and the extracted ISRF fit their corresponding preset curves well. In addition, the average relative error of the extracted IFCF to the preset IFCF is calculated as 0.34% and the average relative error of the extracted ISRF to the preset ISRF is 2.22%. The comparison also confirms the effectiveness of the proposed method in handling such a complicated case.

## 5. Experimental validation

To further test the performance of the proposed method, it is applied to signals collected from experiments. Experiments are conducted on a SpectraQuest machinery fault simulator

(MFS-PK5MT) to collect the bearing vibration signal which is contaminated by interference transmitted from a gearbox and noise. To validate the effectiveness of the proposed method, two different types of signals are collected. In one experiment, the shaft and gearbox are driven by the same motor, i.e. the IFCF is proportional to the gear meshing frequency (fundamental frequency of the interference). In the other experiment, the shaft and gearbox are driven by two different motors, and hence the IFCF and the gear meshing frequency are independent.

### 5.1. Experiment 1: shaft and gearbox driven by the same motor

The set-up of this experiment is shown in Fig. 11. The shaft is supported by two bearings and one of them is a faulty bearing with an outer race fault. The shaft is driven by a motor and the motor is controlled by an AC drive. A gearbox is connected to the shaft by a belt. Parameters of bearings and gears used in this experiment are given in Table 2. The FCC for an outer race fault ( $FCC_O$ ) is calculated as 3.57 by Eq. (10) and the FCC for inner race fault ( $FCC_I$ ) is calculated as 5.43 by Eq. (11). The gear meshing frequency is  $(18/2.6) = 6.92$  times the shaft rotational frequency. A sensor

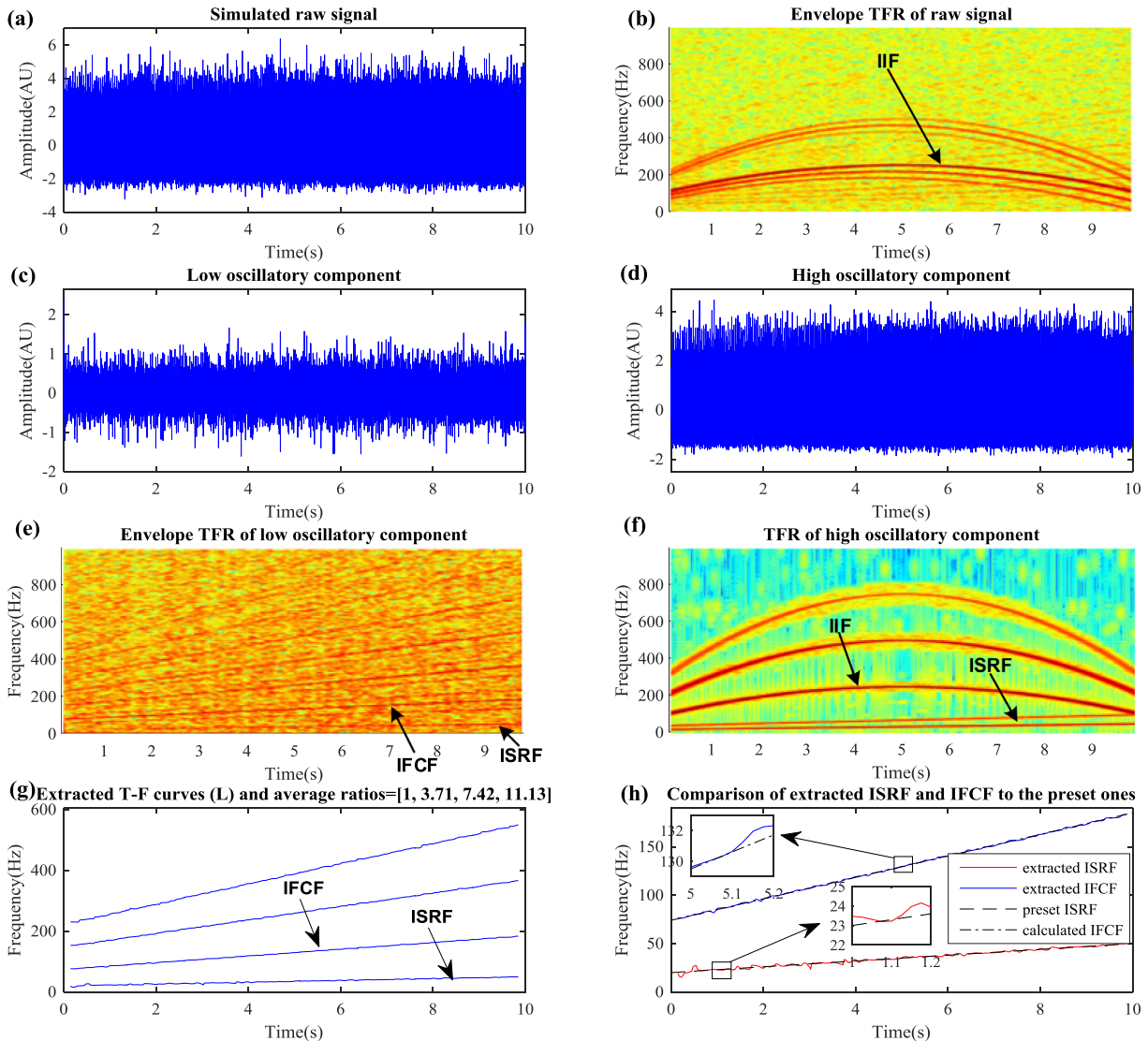


**Fig. 10.** Results of simulation case 4. (a) Simulated raw signal, (b) envelope TFR of raw signal, (c) decomposed low oscillatory component via OBSD, (d) decomposed high oscillatory component, (e) envelope TFR of low oscillatory component, (f) TFR of high oscillatory component, (g) extracted T-F curves from (e), and (h) comparison of extracted ISRF and IFCF to their preset curves.

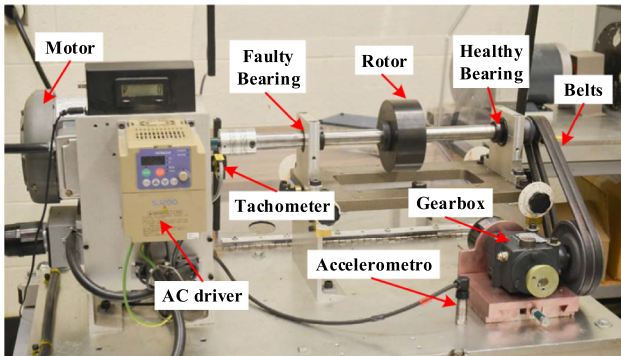


**Fig. 11.** Set-up for Experiment 1.

**Table 2**  
Parameters of bearing and gearbox.

Bearing type	Number of balls	Pitch diameter	Ball diameter	Bearing FCC <sub>O</sub>	Bearing FCC <sub>I</sub>	Diameter ratio of sheaves	Number of gear teeth
ER16K	9	38.52 mm	7.94 mm	3.57	5.43	1:2.6	18

(accelerometer) is mounted on the base of the test rig to collect the vibration signal. Therefore, the collected signal contains not only the bearing vibration signal but also the gear meshing signal. It should be pointed out that to make the fault detection more challenging, the accelerometer is purposely mounted close to the gearbox, yet far away from the shaft supported by the faulty bearing. In this way, the interference effect is enhanced relative to the faulty bearing signal. The signal is sampled by Labview with sampling frequency 20 kHz and the sampling time is 4.46 s. Additionally, to verify the results obtained by the proposed method, a tachometer is used to measure the time-varying shaft rotational speed.

The collected raw signal is shown in Fig. 12(a) and the measured ISRF is shown in Fig. 12(b) which increases from 30.25 Hz to 60.5 Hz. The TFR of the raw signal is obtained via the STFT, as

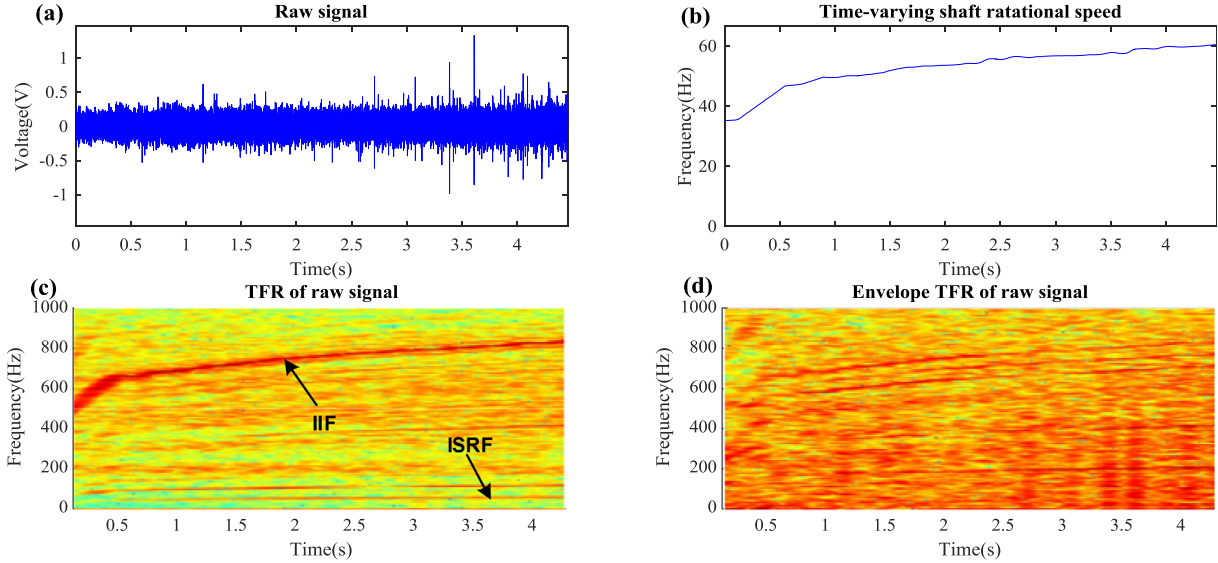


**Fig. 12.** Collected signal of Experiment 1. (a) Collected raw signal, (b) measured ISRF, (c) TFR of the raw signal, and (d) envelope TFR of the raw signal.

shown in Fig. 12(c). It can be seen that the TFR of the raw signal is dominated by the instantaneous gear meshing frequency, i.e. the IIF. The ISRF can also be seen in Fig. 12(c), but the IFCF and its harmonics cannot be observed. Moreover, in the envelope TFR of the raw signal, shown in Fig. 12(d), no clear T-F curves can be observed. Obviously, the bearing fault cannot be detected and diagnosed with the raw signal directly.

According to the proposed method, the OBSD is applied to the raw signal with parameters  $Q_l = 1$ ,  $r_l = 6$ ,  $P_l = 51$ ,  $Q_h = 8$ ,  $r_h = 6$ ,  $P_h = 210$ ,  $\lambda_l = \lambda_h = 0.1$ ,  $\mu = 1$ , and  $K = 250$ . The decomposed low oscillatory component is shown in Fig. 13(a) and the high oscillatory component is shown in Fig. 13(b), respectively. The envelope TFR of the low oscillatory component is obtained via the Hilbert transform and STFT, shown in Fig. 13(c). The IFCF and its harmonics can be observed in Fig. 13(c) without the presence of the IIF and its harmonics. The TFR of the high oscillatory component is also obtained (Fig. 13(d)) in which the IIF and the ISRF can be observed without the IFCF. The results in Fig. 13(c) and (d) demonstrate that the OBSD has effectively separated the bearing fault signature and the interference. Next, the multiple T-F curve extraction algorithm is applied to the envelope TFR of the low oscillatory component, four curves are extracted as shown in Fig. 13(e), and the average ratios are calculated as 1, 1.67, 3.76, and 7.58. However, none of the average ratios match the  $FCC_O$  (3.57) or the  $FCC_I$  (5.43). Hence, according to the proposed method, four additional T-F curves are extracted from the TFR of the high oscillatory component shown in Fig. 13(f) via the multiple T-F curve extraction algorithm. Adding the curve of the lowest frequency in Fig. 13(f)–(e), a new figure of T-F curves is generated shown in Fig. 13(g). Average ratios are re-calculated as 0.94, 1.57, 3.49 and 7.06 by taking the newly added curve as the bottom curve. Among these new average ratios, 3.49 matches the  $FCC_O$  (3.57) with relative error of 2.24% which is within 5%. Thus, the curve of the second highest frequency in Fig. 13(e) is taken as the extracted IFCF and the curve of the lowest curve in Fig. 13(f) is taken as the extracted ISRF. Furthermore, 7.06 matches  $2^* FCC_O$ , which is associated with the 2nd harmonic of the IFCF. Therefore, an outer race fault is diagnosed for the faulty bearing with the proposed method.

For comparison, the extracted ISRF, the measured ISRF, the extracted IFCF and the calculated IFCF are shown in Fig. 13(h). It can be observed that both the ISRF and the extracted IFCF fit the measured curve or the calculated curve quite well. The average relative error of the extracted ISRF to the measured ISRF and

the average relative error of the extracted IFCF to the measured IFCF are calculated as 2.54% and 2.32%, respectively.

## 5.2. Experiment 2: shaft and gearbox driven by different motors

In this case, the set-up of the experiment is shown in Fig. 14. The only difference from the first experiment (Fig. 11) is that the gearbox is connected to another shaft driven by another motor, labeled as motor 2 in Fig. 14. Thus, the gear meshing frequency is 6.92 times of the rotational frequency of the shaft that the gearbox connects to. The  $FCC_O$  (3.57) and the  $FCC_I$  (5.43) are the same since the bearings are the same. Once again, the accelerometer is intentionally placed in the vicinity of the gearbox but far away from the faulty bearing so that the interference signal will be more pronounced. The sampling frequency is 20 kHz and the sampling time is 6.23 s.

The collected raw signal is shown in Fig. 15(a) and the measured ISRF of the shaft supported by the faulty bearing is shown in Fig. 15(b) which rises almost linearly from 23 Hz to 36 Hz. The TFR of the raw signal is shown in Fig. 15(c). Similarly, the TFR is dominated by the IIF (gear meshing frequency) and the ISRF also appears. The envelope TFR of the raw signal is shown in Fig. 15(d), in which only the IIF and its harmonics can be observed. It can be seen that in both Fig. 15(c) and (d), the IFCF and its harmonics are absent which again indicates that the bearing fault cannot be directly detected from the raw signal.

To extract the bearing fault signature from the obscured raw signal, the OBSD is applied to the raw signal with parameters  $Q_l = 1$ ,  $r_l = 6$ ,  $P_l = 51$ ,  $Q_h = 9$ ,  $r_h = 6$ ,  $P_h = 251$ ,  $\lambda_l = \lambda_h = 0.1$ ,  $\mu = 2$ , and  $K = 200$ . The obtained low oscillatory component and the high oscillatory component are shown in Fig. 16(a) and (b), respectively. The envelope TFR of the low oscillatory component is displayed in Fig. 16(c). The IFCF and its 2nd harmonic can be clearly observed without the presence of the IIF, which implies that the bearing fault signature is effectively extracted as the low oscillatory component. Additionally, the TFR of the high oscillatory component is shown in Fig. 16(d) where only the IIF and the ISRF can be observed, without the presence of the IFCF, which indicates that the OBSD has successfully separated the bearing fault signature and the interference. According to the proposed method, four T-F curves are extracted from the TFR, shown in Fig. 16(c), via the multiple T-F curve extraction algorithm. The extracted T-F curves are shown in Fig. 16(e). The calculated average ratios for the four

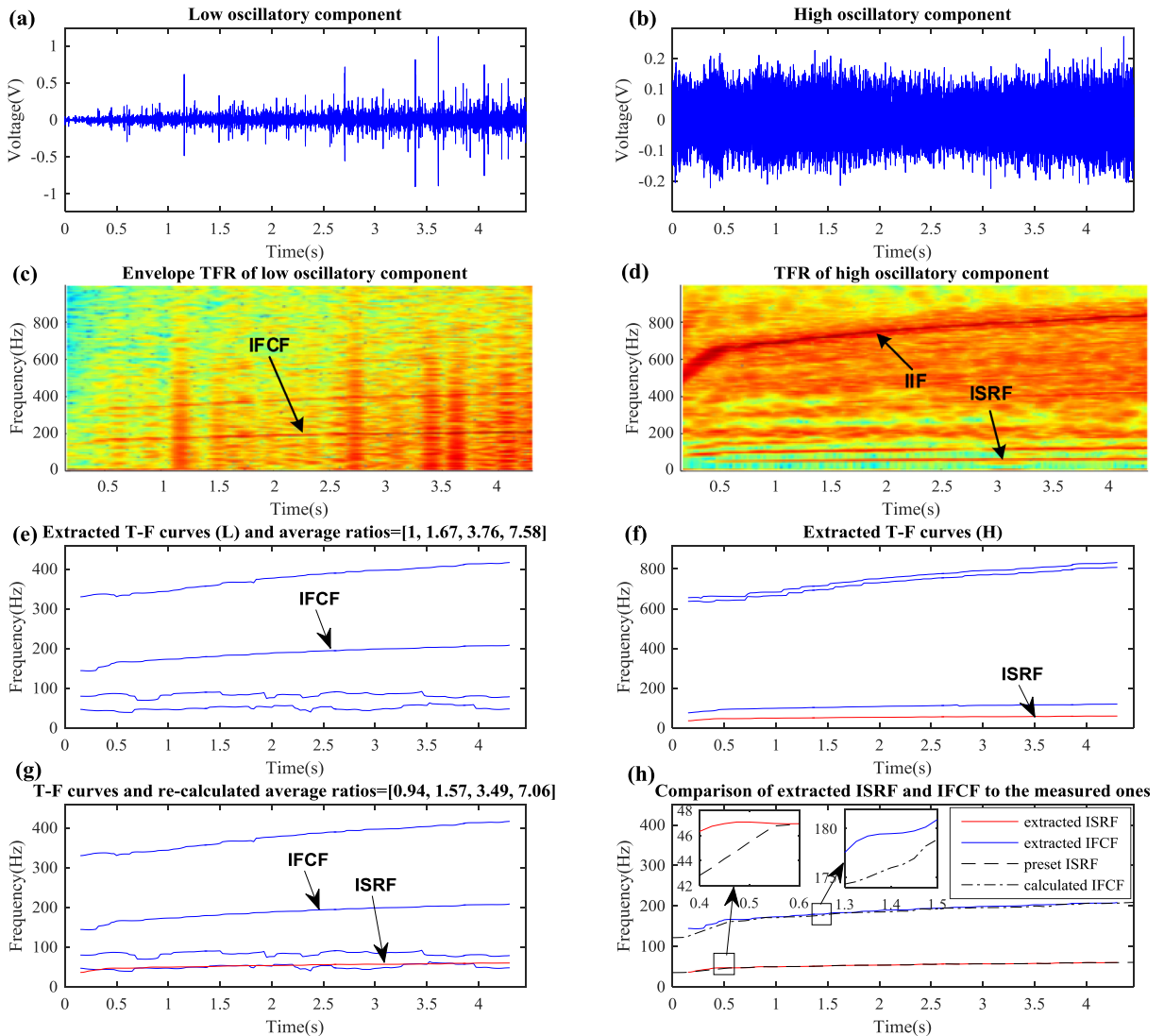


**Fig. 13.** Results of Experiment 1. (a) Decomposed low oscillatory component via OBSD, (b) decomposed high oscillatory component, (c) envelope TFR of low oscillatory component, (d) TFR of high oscillatory component, (e) extracted T-F curves from (c), (f) extracted T-F curves from (d), (g) T-F curves used for bearing fault diagnosis, and (h) comparison of extracted ISRF and IFCF to their preset curves.

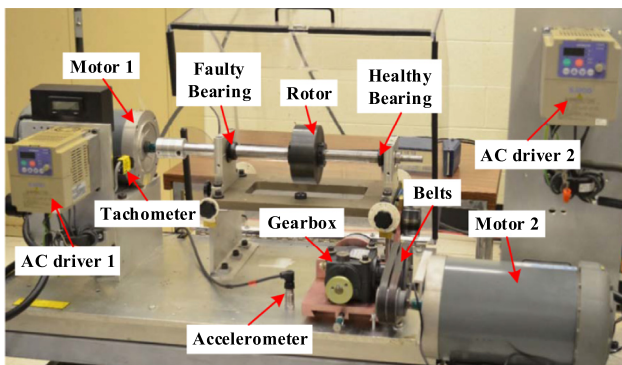
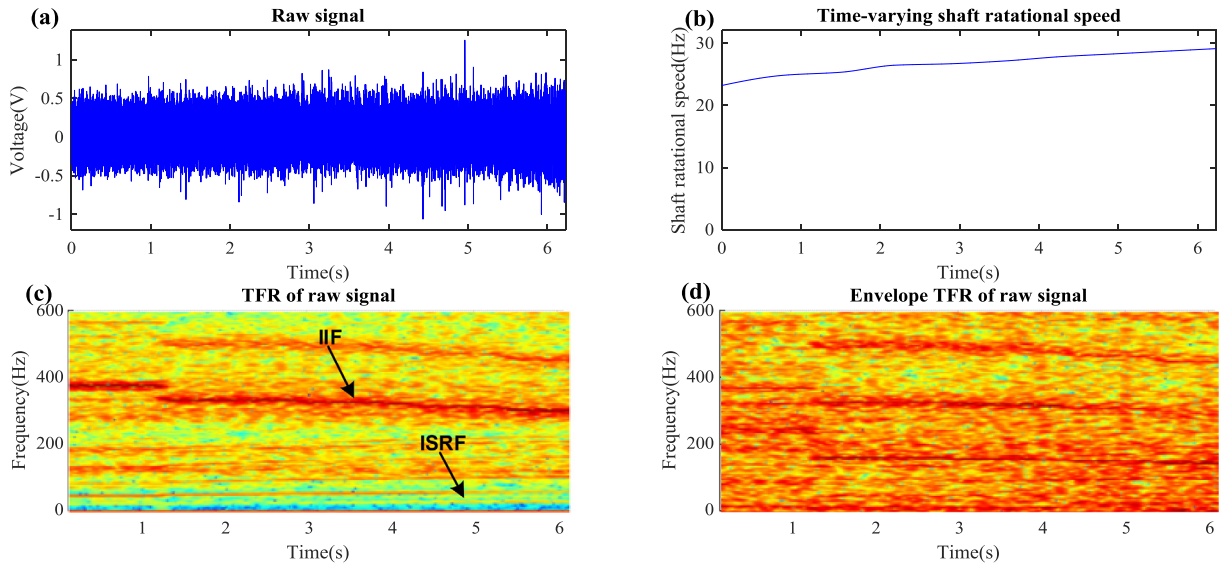


**Fig. 14.** Set-up of Experiment 2.

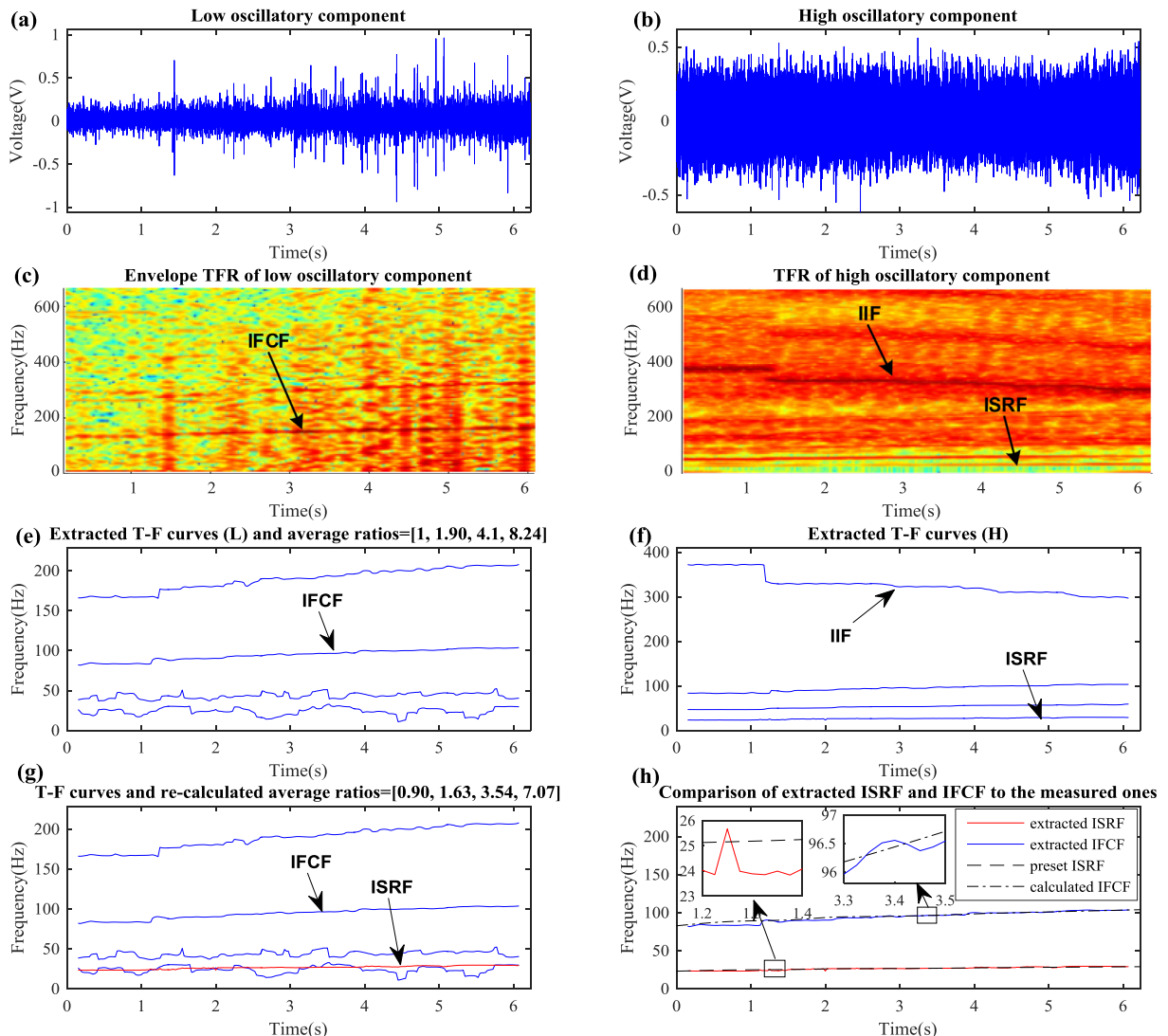
curves are 1, 1.90, 4.10 and 8.24, respectively. None of them match the  $FCC_0$  (3.57) or the  $FCC_1$  (5.43) since the ISRF is not present in Fig. 16(c). Thus, another four curves are extracted (shown in Fig. 16(f)) from the TFR shown in Fig. 16(d), in accordance with the proposed method. A new figure is generated, shown in

Fig. 16(g), by adding the curve with the lowest frequency in Fig. 16(f) to the T-F curves in Fig. 16(f). By taking the newly added curve as the bottom curve, the average ratios of the four other curves in Fig. 16(g) are calculated as 0.90, 1.63, 3.54 and 7.07. Among these average ratios, 3.54 matches the  $FCC_0$  (3.57) with relative error of 0.84% (within 5%). Therefore, the new bottom curve and the second highest curve in Fig. 16(g) are treated as the extracted ISRF and the extracted IFCF, respectively. In addition, 7.07 matches  $2^* FCC_0$  which indicates that the highest curve in Fig. 16(e) is the 2nd harmonic of the IFCF. Hence, the bearing is diagnosed as faulty with an outer race fault via the proposed method.

To further demonstrate the performance of the proposed method, a comparison figure of the extracted ISRF to the measured ISRF and the extracted IFCF to the calculated IFCF is shown in Fig. 16(h). Similarly, it can be seen that both the extracted ISRF and the extracted IFCF fit the measured curve or the calculated curve. Also, the average relative error of the extracted ISRF to the measured ISRF and the average relative error of the extracted IFCF to the calculated IFCF are calculated as 2.04% and 1.53%, respectively, which confirms the effectiveness of the proposed method.



**Fig. 15.** Collected signal of Experiment 2. (a) Collected raw signal, (b) measured ISRF, (c) TFR of the raw signal, and (d) envelope TFR of the raw signal.



**Fig. 16.** Results of Experiment 2. (a) Decomposed low oscillatory component via OBSD, (b) decomposed high oscillatory component, (c) envelope TFR of low oscillatory component, (d) TFR of high oscillatory component, (e) extracted T-F curves from (c), (f) extracted T-F curves from (d), (g) T-F curves used for bearing fault diagnosis, and (h) comparison of extracted ISRF and IFCF to their preset curves.

## 6. Conclusions

In this paper, a methodology for resampling-free and tachometer-free bearing fault diagnosis under time-varying speed conditions in the presence of an interference signal was proposed based on the oscillatory behavior of the signal. The proposed method implements the OBSD to extract the bearing fault signature from the contaminated signal. Then, an IFCF&ISRF search algorithm is utilized to estimate the IFCF and ISRF from the TFR of the processed signal. Finally, the bearing fault is identified based on the average curve-to-curve ratio of the estimated IFCF/ISRF. The proposed IFCF&ISRF search algorithm is able to estimate the ISRF, even if the shaft rotating frequency is not included in the extracted bearing fault signature via the OBSD.

The performance of the proposed method is validated by simulated signals and experimental data. The simulated signals are four signals with different settings, including cases where the simulated IFCF and IIF do/do not cross each other and the ISRF is/is not modulated by the bearing fault-induced signal. The experimental data are collected from two experiments conducted under different conditions. In the first experiment, the shaft and gearbox (interference resource) are driven by the same motor while in the second experiment, they are driven by two different motors. The results of all four simulations and two experiments demonstrate that the proposed method can be used for effective bearing fault diagnosis under time-varying speed conditions in the presence of interference, without using tachometers.

## Acknowledgements

This work was financially supported by the Natural Sciences and Engineering Research Council of Canada (RGPIN-2016-04190, RGPIN/121433), the Ontario Centers of Excellence (OT-SE-E50622) and the China Scholarships Council. The authors would also like to thank Dr. T. Wang for the data collected in our lab at the University of Ottawa.

## References

- [1] P.D. McFadden, J.D. Smith, Vibration monitoring of rolling element bearings by the high-frequency resonance technique—a review, *Tribol. Int.* 17 (1984) 3–10.
- [2] J. Shiroishi, Y. Li, S. Liang, T. Kurfess, S. Danyluk, Bearing condition diagnostics via vibration and acoustic emission measurements, *Mech. Syst. Signal Process.* 11 (1997) 693–705.
- [3] D. Brie, Modelling of the spalled rolling element bearing vibration signal: an overview and some new results, *Mech. Syst. Signal Process.* 14 (2000) 353–369.
- [4] R.B. Randall, J. Antoni, Rolling element bearing diagnostics—a tutorial, *Mech. Syst. Signal Process.* 25 (2011) 485–520.
- [5] A. Glowacz, W. Glowacz, Z. Glowacz, J. Kozik, Early fault diagnosis of bearing and stator faults of the single-phase induction motor using acoustic signals, *Measurement* 113 (2018) 1–9.
- [6] A. Glowacz, Acoustic based fault diagnosis of three-phase induction motor, *Appl. Acoust.* 137 (2018) 82–89.
- [7] A. Glowacz, Fault diagnosis of single-phase induction motor based on acoustic signals, *Mech. Syst. Signal Process.* 117 (2019) 65–80.
- [8] Y. Guo, T.W. Liu, J. Na, R.F. Fung, Envelope order tracking for fault detection in rolling element bearings, *J. Sound Vib.* 331 (2012) 5644–5654.
- [9] P. Borghesani, R. Ricci, S. Chatterton, P. Pennacchi, A new procedure for using envelope analysis for rolling element bearing diagnostics in variable operating conditions, *Mech. Syst. Signal Process.* 38 (2013) 23–35.
- [10] K.M. Bossley, R.J. Kendrick, C.J. Harris, C. Mercer, Hybrid computed order tracking, *Mech. Syst. Signal Process.* 13 (1999) 627–641.
- [11] K.R. Fyfe, E.D.S. Munck, Analysis of computed order tracking, *Mech. Syst. Signal Process.* 11 (1997) 187–205.
- [12] Z. Feng, M. Liang, F. Chu, Recent advances in time-frequency analysis methods for machinery fault diagnosis: A review with application examples, *Mech. Syst. Signal Process.* 38 (2013) 165–205.
- [13] S. Olhede, A.T. Walden, A generalized demodulation approach to time-frequency projections for multicomponent signals, *Proc. R. Soc. A Math. Phys. Eng. Sci.* 461 (2005) 2159–2179.
- [14] Z. Feng, X. Chen, M. Liang, Joint envelope and frequency order spectrum analysis based on iterative generalized demodulation for planetary gearbox fault diagnosis under nonstationary conditions, *Mech. Syst. Signal Process.* 76–77 (2015) 242–264.
- [15] J. Shi, M. Liang, Y. Guan, Bearing fault diagnosis under variable rotational speed via the joint application of windowed fractal dimension transform and generalized demodulation: A method free from prefiltering and resampling, *Mech. Syst. Signal Process.* 68–69 (2016) 15–33.
- [16] T. Wang, M. Liang, J. Li, W. Cheng, Rolling element bearing fault diagnosis via fault characteristic order (FCO) analysis, *Mech. Syst. Signal Process.* 45 (2014) 139–153.
- [17] M. Zhao, J. Lin, X. Xu, Y. Lei, Tacholess envelope order analysis and its application to fault detection of rolling element bearings with varying speeds, *Sensors* 13 (2013) 10856–10875.
- [18] Y. Wang, G. Xu, A. Luo, L. Liang, K. Jiang, An online tacholess order tracking technique based on generalized demodulation for rolling bearing fault detection, *J. Sound Vib.* 367 (2016) 233–249.
- [19] J. Antoni, The spectral kurtosis: A useful tool for characterising non-stationary signals, *Mech. Syst. Signal Process.* 20 (2006) 282–307.
- [20] J. Antoni, R.B. Randall, The spectral kurtosis: application to the vibratory surveillance and diagnostics of rotating machines, *Mech. Syst. Signal Process.* 20 (2006) 308–331.
- [21] T. Wang, M. Liang, J. Li, W. Cheng, C. Li, Bearing fault diagnosis under unknown variable speed via gear noise cancellation and rotational order sideband identification, *Mech. Syst. Signal Process.* 62 (2015) 30–53.
- [22] I.W. Selesnick, Resonance-based signal decomposition: a new sparsity-enabled signal analysis method, *Signal Processing* 91 (2011) 2793–2809.
- [23] L. Cui, D. Mo, H. Wang, P. Chen, Resonance-based nonlinear demodulation analysis method of rolling bearing fault, *Adv. Mech. Eng.* 5 (2013) 1–13.
- [24] J. Shi, M. Liang, Intelligent bearing fault signature extraction via iterative oscillatory behavior based signal decomposition (IOBSD), *Expert Syst. Appl.* 45 (2016) 40–55.
- [25] H. Huang, N. Baddour, M. Liang, Auto-OBSD: automatic parameter selection for reliable oscillatory behavior-based signal decomposition with an application to bearing fault signature extraction, *Mech. Syst. Signal Process.* 86 (2017) 237–259.
- [26] R.B. Randall, *Vibration-based Condition Monitoring: Industrial, Aerospace and Automotive Applications*, John Wiley & Sons, 2011.
- [27] R. Yan, R.X. Gao, Hilbert-huang transform-based vibration signal analysis for machine health monitoring, *IEEE Trans. Instrum. Meas.* 55 (2006) 2320–2329.
- [28] L.D. Meyer, F.F. Ahlgren, B. Weichbrodt, An analytic model for ball bearing vibrations to predict vibration response to distributed defects, *J. Mech. Des.* 102 (1980) 205–210.
- [29] I.W. Selesnick, Wavelet transform with tunable Q-factor, *IEEE Trans. Signal Process.* 59 (2011) 3560–3575.
- [30] H. Huang, N. Baddour, M. Liang, Bearing fault diagnosis under unknown time-varying rotational speed conditions via multiple time-frequency curve extraction, *J. Sound Vib.* 414 (2018).
- [31] D. Iatsenko, P.V.E. Mcclintock, A. Stefanovska, Extraction of instantaneous frequencies from ridges in time – frequency representations of signals, *Signal Processing* 125 (2016) 290–303.